REPORT DOCUMENTATION PAGE

Form Approved OMB NO. 0704-0188

1. REPORT DATE (DD-MM-YYYY)	2. REPORT TYPE	3. DATES COVERED (From - To)
13-03-2012	Final Report	3-Sep-2009 - 2-Jul-2011

4. TITLE AND SUBTITLE

FINAL REPORT - contract No. W911NF-09-C-0135
Part I. Developing Sensitive and Selective Nanosensors: A Single Molecule - Multiple Excitation Source Approach
Part II. Altairnano Lithium Ion Nano-scaled Titanate Oxide Cell and Module Abuse Testing

5a. CONTRACT NUMBER

5b. GRANT NUMBER
W911NF-09-C-0135

5c. PROGRAM ELEMENT NUMBER
106013

6. AUTHORS
Michael Coleman, Thushara Gunasinghe, Lisa Kennedy, Michael Reed, Dave Miller

5d. PROJECT NUMBER

5e. TASK NUMBER

5f. WORK UNIT NUMBER

7. PERFORMING ORGANIZATION NAMES AND ADDRESSES
Altairnano, Inc.
204 Edison Way
Reno, NV 89502 -

8. PERFORMING ORGANIZATION REPORT NUMBER

9. SPONSORING/MONITORING AGENCY NAME(S) AND ADDRESS(ES)
U.S. Army Research Office
P.O. Box 12211
Research Triangle Park, NC 27709-2211

10. SPONSOR/MONITOR'S ACRONYM(S)
ARO

11. SPONSOR/MONITOR'S REPORT NUMBER(S)
55328-CH.1

12. DISTRIBUTION AVAILIBILITY STATEMENT
Approved for Public Release; Distribution Unlimited

13. SUPPLEMENTARY NOTES
The views, opinions and/or findings contained in this report are those of the author(s) and should not contrued as an official Department of the Army position, policy or decision, unless so designated by other documentation.

14. ABSTRACT
This final report for Contract W911NF-09-C-0135 transmits the findings of research on two topics.

The first (Part I.)is "Developing Sensitive and Selective Nanosensors". The partnership of Altairnano, Inc. and Western Michigan University produced one compound which could be used to identify nerve gas analogs selectively in the presence of fuel-based interference compounds. This research developed the framework for a

15. SUBJECT TERMS
Nanosensor, Nerve Gas Sensors, Lithium Ion Cells, Abuse Testing, Battery Testing

16. SECURITY CLASSIFICATION OF:			17. LIMITATION OF ABSTRACT	15. NUMBER OF PAGES	19a. NAME OF RESPONSIBLE PERSON
a. REPORT	b. ABSTRACT	c. THIS PAGE			Bruce Sabacky
UU	UU	UU	UU		19b. TELEPHONE NUMBER: 775-858-3766

Report Title

FINAL REPORT - contract No. W911NF-09-C-0135
Part I. Developing Sensitive and Selective Nanosensors: A Single Molecule - Multiple Excitation Source Approach
Part II. Altairnano Lithium Ion Nano-scaled Titanate Oxide Cell and Module Abuse Testing

ABSTRACT

This final report for Contract W911NF-09-C-0135 transmits the findings of research on two topics.

The first (Part I.)is "Developing Sensitive and Selective Nanosensors". The partnership of Altairnano, Inc. and Western Michigan University produced one compound which could be used to identify nerve gas analogs selectively in the presence of fuel-based interference compounds. This research developed the framework for a prototype sensor which can be easily augmented to demonstrate function based on sensing requirments. The research described in the final report consists of sensor selection, sample preparation, library development and analysis, and prototype development.

The second (Part II.) is "Altairnano Lithium Ion Nano-scaled Titanate Oxide Cell and Module Abuse Test Report". The partnership of Altairnano, Inc. and the Naval Surface Warfare Center in Crane, Indiana produced a set of abuse test results which could be used to evaluate the use of Altairnano's lithium ion cells in US Army applications such as the M119/105mm Gun batteries. The abuse testing focused on exposure to extreme heat and flame, on the analysis of gases released due to exposure, and on fire suppression methods.

Enter List of papers submitted or published that acknowledge ARO support from the start of the project to the date of this printing. List the papers, including journal references, in the following categories:

(a) Papers published in peer-reviewed journals (N/A for none)

Received Paper

TOTAL:

Number of Papers published in peer-reviewed journals:

(b) Papers published in non-peer-reviewed journals (N/A for none)

Received Paper

TOTAL:

Number of Papers published in non peer-reviewed journals:

(c) Presentations

Number of Presentations:

Non Peer-Reviewed Conference Proceeding publications (other than abstracts):

Received Paper

TOTAL:

Number of Non Peer-Reviewed Conference Proceeding publications (other than abstracts):

Peer-Reviewed Conference Proceeding publications (other than abstracts):

Received Paper

TOTAL:

Number of Peer-Reviewed Conference Proceeding publications (other than abstracts):

(d) Manuscripts

Received Paper

TOTAL:

Number of Manuscripts:

Books

Received Paper

TOTAL:

Patents Submitted

Patents Awarded

Awards

Graduate Students

NAME	PERCENT_SUPPORTED
FTE Equivalent:	
Total Number:	

Names of Post Doctorates

NAME	PERCENT_SUPPORTED
FTE Equivalent:	
Total Number:	

Names of Faculty Supported

NAME	PERCENT_SUPPORTED
FTE Equivalent:	
Total Number:	

Names of Under Graduate students supported

NAME	PERCENT_SUPPORTED
FTE Equivalent:	
Total Number:	

Student Metrics

This section only applies to graduating undergraduates supported by this agreement in this reporting period

The number of undergraduates funded by this agreement who graduated during this period: .....

The number of undergraduates funded by this agreement who graduated during this period with a degree in science, mathematics, engineering, or technology fields:.....

The number of undergraduates funded by your agreement who graduated during this period and will continue to pursue a graduate or Ph.D. degree in science, mathematics, engineering, or technology fields:.....

Number of graduating undergraduates who achieved a 3.5 GPA to 4.0 (4.0 max scale): .....

Number of graduating undergraduates funded by a DoD funded Center of Excellence grant for Education, Research and Engineering: .....

The number of undergraduates funded by your agreement who graduated during this period and intend to work for the Department of Defense .....

The number of undergraduates funded by your agreement who graduated during this period and will receive scholarships or fellowships for further studies in science, mathematics, engineering or technology fields: .....

Names of Personnel receiving masters degrees

NAME
Total Number:

Names of personnel receiving PHDs

NAME
Total Number:

Names of other research staff

NAME	PERCENT_SUPPORTED
FTE Equivalent:	
Total Number:	

Sub Contractors (DD882)

1 a. Western Michigan University

1 b. Western Michigan University
1903 West Michigan Avenue
Kalamazoo MI 49008

Sub Contractor Numbers (c): N/A

Patent Clause Number (d-1): N/A

Patent Date (d-2):

Work Description (e): The Chemistry Dept. of WMU worked with Altairnano to develop and synthsize sensor molecules f

Sub Contract Award Date (f-1):

Sub Contract Est Completion Date(f-2):

---

1 a. Western Michigan University

1 b. A223 Elsworth Hall
Kalamazoo MI 49008

Sub Contractor Numbers (c): N/A

Patent Clause Number (d-1): N/A

Patent Date (d-2):

Work Description (e): The Chemistry Dept. of WMU worked with Altairnano to develop and synthsize sensor molecules f

Sub Contract Award Date (f-1):

Sub Contract Est Completion Date(f-2):

Inventions (DD882)

Scientific Progress

Technology Transfer

FINAL REPORT

Contract No. W911NF-09-C-0135

Principal Investigator: Bruce J. Sabacky

Abstract

This final report for Contract W911NF-09-C-0135 transmits the findings of research on two topics.

The first (Part I.) is "Developing Sensitive and Selective Nanosensors" A Single Molecule – Multiple Excitation Source Approach. The partnership of Altairnano, Inc. and Western Michigan University produced one compound which could be used to identify nerve gas analogs selectively in the presence of fuel-based interference compounds. This research developed the framework for a prototype sensor which can be easily augmented to demonstrate function based on sensing requirments. The research described in the final report consists of sensor selection, sample preparation, library development and analysis, and prototype development.

The second (Part II.) is "Altairnano Lithium Ion Nano-scaled Titanate Oxide Cell and Module Abuse Test Report". The partnership of Altairnano, Inc. and the Naval Surface Warfare Center in Crane, Indiana produced a set of abuse test results which could be used to evaluate the use of Altairnano's lithium ion cells in US Army applications such as the M119/105mm Gun batteries. The abuse testing focused on exposure to extreme heat and flame, on the analysis of gases released due to exposure, and on fire suppression methods.

FINAL REPORT

Contract No. W911NF-09-C-0135

Part I. Developing Sensitive and Selective Nanosensors: A Single Molecule – Multiple Excitation Source Approach

Authors: Michael Coleman, Thushara Gunasinghe, and Lisa Kennedy

Introduction

The partnership of Altair and Western Michigan University has been working on the problem of identification of nerve gas molecules for several years, and over that time we have developed many compounds which can be used for identifying nerve gasses. In this phase of the project we have been working to expand our efforts in order to produce a functioning prototype which takes into account the interaction of the sensing molecules with the environment. Cost, reliability and sensitivity were examined and a preliminary design was set wherein a disposable gel affixed sensor array would be inserted into a reusable low cost optic device. Our work towards these efforts can be described then as sensor selection, sample preparation, library development and analysis, and prototype development.

Sensor Selection

In addition to the nerve gas analogs which we have primarily focused on in the past our list of target molecules has expanded to look for possible interference compounds and to a lesser extent other toxic industrial chemicals. It is unlikely in this complex system that a single sensing molecule will be developed which will have both the sensitivity and the selectivity that is needed. Therefore a list of compounds has been gathered which should yield a rough description of the chemical nature of the analytes. Using 14 samples provided by Western Michigan University we have supplemented with compounds developed at Altair and then added a large number of commercially available sensing compounds to provide further structural information on the incoming analytes. Each dye was then scanned using a UV-Vis Spectrometer to find the optimal exposure wavelengths. Following this exposure a concentration study was conducted to find the most appropriate concentration of the dyes in our experiments.

List of Sensing Compounds

Name	Source	Amount Dissolved	Specifications
1	WMU	4920ppm in EtOH	NA
2	WMU	4625ppm in EtOH	NA
3	WMU	120ppm in EtOH	NA
4	WMU	260ppm in EtOH	NA
5	WMU	100ppm in EtOH	NA
6	WMU	900ppm in EtOH	NA

7	WMU	4500ppm in EtOH	NA
A	WMU	1450ppm in EtOH	NA
B	WMU	600ppm in EtOH	NA
C	WMU	250ppm in EtOH	NA
D	WMU	450ppm in EtOH	NA
E	WMU	450ppm in EtOH	NA
F	WMU	300ppm in EtOH	NA
Fluoresceinamine		250ppm in DMSO	Isomer 1, Sigma Aldrich, $C_{20}H_{13}NO_5$
Thymol Blue		200ppm in EtOH	JT Baker, $C_{27}H_{30}O_5S$, Transitions from Red to yellow when acidic and yellow to blue when basic.
Nile Red		20ppm in DMSO	Fluka Analytical, $C_{20}H_{18}N_2O_2$, Red lipophilic stain.
N,N'-Dimethyl-9,9'-biacridium dinitrate		630ppm in EtOH	Sigma-Aldrich, $C_{28}H_{22}N_4O_6$, Lucigenin, bluish-green fluorescence.
5,5'-Dithiobis(2-nitrobenzoic acid)		390ppm in EtOH	Sigma Life Sciences, $[-SC_6H_3(NO_2)CO_2H]_2$, bioreagent suitable for determination of sulfhydryl groups.
Terbium Melamine		6013ppmin EtOH	NA
Silver Terpyridine		120ppm in EtOH	NA
Coumarin-1		62.5ppm in EtOH	Pure, laser grade, ARCOS ORGANICS, $C_{14}H_{17}NO_2$
Melamine (Eu/Tb/Sm/Dy)		9067ppm in EtOH	NA
Melamine (Eu/Tb/Dy/Sm)		4000ppm in EtOH	NA
Melamine $(EuLotd)_3$/Tb/Sm/Dy		760ppm in EtOH	NA
Coumarin-152		1000ppm in EtOH	$C_{12}H_{10}F_3NO_2$
Coumarin-334		125ppm in EtOH	99% Pure, laser grade, ARCOS ORGANICS
Coumarin-6		62.5ppm in EtOH	98% Pure, laser grade, ARCOS ORGANICS, $C_{20}H_{18}N_2O_2S$
Coumarin-7		62.5ppm in EtOH	$C_{20}H_{19}N_3O_2$
H-Porphine		125ppm in EtOH	NA
Fuschin Hydrochloride		20ppm in EtOH	MP Biomedicals, LLC, $C_{20}H_{19}N_3 \cdot HCl$, Purple to red dye
Bromocresol Green		690ppm in EtOH	Fisher Scientific, $C_{21}H_{14}Br_4O_5S$, Light brown when acidic or dark green when basic.
Congo Red		28.8ppm in EtOH	RICCA Chemical Company, 0.5% (w/v) in 10% (v/v) alcohol, $C_{32}H_{22}N_6Na_2O_6S_2$, Red solution.
Methyl Red		200ppm in EtOH	Alfa Aesar, $C_{15}H_{15}N_3O_2$, Red in acidic solution and yellow in basic solution.
Methylene Blue Chloride		610ppm in EtOH	Matheson Coleman & Bell, $C_{16}H_{18}ClN_3S$, Dark green powder that yields blue solution.
Eosin B		200ppm in EtOH	Certified, 90% Sigma Aldrich, $C_{20}H_8Br_2N_2O_9$; Fluorescent red dye.
Chromotrope 2B		390ppm in EtOH	Fluka Analytical, $C_{16}H_9N_3O_{10}S_2Na_2$ Acid Red
$(26P_4Acid)Eu\text{-}SiO_2$		7825ppm in EtOH	NA
$(36P_4)(SiO_2)(Eu)$		1750ppm in EtOH	NA
$4(6P_4Acid)\text{-}SiO_2\text{-}Eu$		8100ppm in DMSO	NA
8	WMU	400ppm in EtOH	NA
9	WMU	400ppm in EtOH	NA
OBARE	WMU	440ppm in EtOH	NA
G	WMU	200ppm in EtOH	NA
H	WMU	200ppm in EtOH	NA

Sample Preparation

The sensitivity of our system is based on the interaction of the analyte molecule with the sensing molecule. To aid in this process all of the sensing molecules have to be exposed to the incoming analyte molecule. This could be accomplished with an open structure with very high surface area covered in a dry monolayer of sensing compound, a scenario which is both difficult to achieve and yields a large amount of noise from light scattering. Another alternative would be to place the dye dissolved into a liquid medium where the incoming analyte can interact freely with the bulk of the dye molecules. A liquid medium also has the benefit of trapping analyte molecules, as once they have entered the solution the residence time in proximity to the sensing molecules is increased. A liquid sample would be ideal if it were not for the implementation in the field, in which a liquid sample adds complexity to an already complex system. Fortunately similar characteristics can be achieved by dispersing the dye compound in a gel medium.

Multiple systems of gels were examined to provide a porous substrate that could be easily transferred to the multiwall plates. Gels analyzed included agarose, gelatin, poly(vinyl alcohol), and poly(2-hydroxyethyl methacrylate). Agarose and gelatin did not produce gels which were rigid enough and also had a very open pore structure which led to leaching of the dye, which is undesirable in the printed sensor matrix. A cured HEMA gel resembled glass and was not porous and was disregarded. PVA proved to be the best candidate and a 30 wt % gel looked to be close to the properties desired in the finished product. The preparation of this gel however produced a highly viscous solution which made metering difficult. For convenience a 5 wt% solution was used as this would give a good idea of the interaction of dyes and analytes with the gel but still allow convenient handling in sample preparation.

The first attempts to develop a PVA gel involved a various percentages of PVA in a 50:50 water:DMSO matrix using high heat and high shear. These batches did not result in a homogenous gel and a new approach was taken, using only water as the matrix. The percentage of PVA in water was varied in order to find the strongest pipettable gel solution. The chosen method incorporated a solution of 5% PVA (Acros Organics, poly(vinyl alcohol), 95% hydrolyzed, average M.W. 95000) in deionized water with constant stirring and heat. 100µL of this mixture was pipetted into each well of a 96-well plate (BD Falcon Microtest 96-well Assay Plate, Optilux Black/Clear bottom, TC Surface) using a muliti-well pippetter (Research Eppendorf 100). Once prepared, these plates were degassed in a sonicating bath for 5 minutes and placed in a freezer (-25ºC) for 4 hours. After the freeze cycle, the plates are removed and allowed to thaw for at least 4 hours prior to addition of dyes.

Forty-four dyes were chosen based on their structures and if a color change would be evident after exposure to certain analytes. A series of dilutions of each dye in ethanol (some required DMSO as they weren't soluble in ethanol) were performed and run on a UV/Vis Spectrophotometer (Beckman DU 520) and analyzed using DU 500.HT in order to obtain an ideal concentration to fill the wells. Each dye was then added to two wells, spatially separated to reduce noise from gas mixing in the chamber, on the plate see

figure 1. Once the plates were filled with the designated dyes, they were topped with parafilm and lids and placed in the refrigerator for preservation. Only ten plates were made at a time to prevent dehydration, as time constraints limit testing to only one plate per day.

	1	**2**	**3**	**4**	**5**	**6**	**7**	**8**	**9**	**10**	**11**	**12**
A	1	2	3	4	5	6	1	2	3	4	5	6
B	7	A	B	C	D	E	7	A	B	C	D	E
C	F	FC	TB	NR	NN'	55'	F	FC	TB	NR	NN'	55'
D	TbMe	AgT	C1	mla Eu:Tb: Sm:Dy	mla Eu:Tb: Dy:Sm	mla Eu(Lotd) (Tb)(Sm)(Dy)	TbMe	AgT	C1	mla Eu:Tb: Sm:Dy	mla Eu:Tb: Dy:Sm	mla Eu(Lotd) (Tb)(Sm)(Dy)
E	C152	C334	C6	C7	HP	FH	C152	C334	C6	C7	HP	FH
F	BCG	CR	MR	MBC	EB	CH	BCG	CR	MR	MBC	EB	CH
G	26P4	36P4	46P4	8	9	OBARE	26P4	36P4	46P4	8	9	OBARE
H	G	H	Blank	Blank	Blank	Blank	G	H	Blank	Blank	Blank	Blank

Figure 1. Multiwell Plate layout

Initial scans without the lid were made using a Vis Spectrophotometer Plate Reader (Biotek Instruments Elx800) at 450nm, 490nm, 562nm, 630nm, and 690nm. These results were analyzed via Gen5 1.09. As the Vis spectrometer reading was complete in under 5 minutes it was possible to perform the scan without a cover and little change could be expected from evaporation, however with the fluorescent readings this measurement was roughly three and a half hours and to keep the sample response the plate was sealed during this reading. A microwell plate reader (Micromax 384 Microwell Plate Reader Horiba Jobin Yvon) in conjunction with a flourimeter (Fluorolog Horiba Jobin Yvon and SpectraQ Horiba Jobin Yvon) were used to scan the plate at various excitations. The excitations used were 300nm, 330nm, 380nm, and 450nm. The software used to analyze the data was FluorEssence Horiba Jobin Yvon 2005.

Once the initial tests are completed, the plate is transported to an exposure chamber without the lid. This chamber is then sealed, and a chosen analyte is distributed through the chamber for 15 minutes. The ratio of analyte to air could be adjusted to have a lower concentration or a higher concentration of analyte. Once exposure was complete, a gas sample was collected in a sample bag (SKC Quality Sample Bag, 0.5L 36435). The contents of this bag were later analyzed via titrations and the GCMS.

For these exposures two plates were run for each analyte; one at a high concentration and one at a low concentration. The first flowmeter is adjusted to 0.8 ft^3/hr and the second to 0.2 ft^3/hr for a low concentration and 0.7 ft^3/hr and 0.3 ft^3/hr respectively for a high concentration of analyte. To test the effect of an interference compound on the response of the sensing molecules the system was modified to allow a second gas stream to be added. Schematics for the two setups are shown in figures 2 and 3.

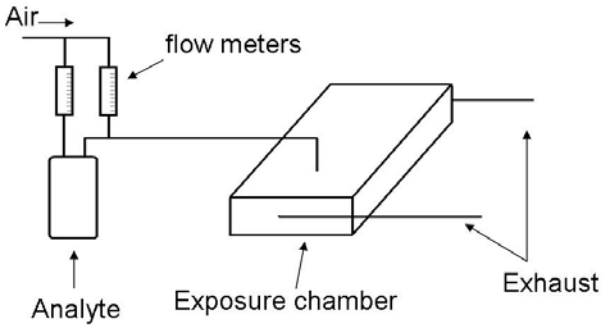

Figure 2. Single analyte gas exposure system.

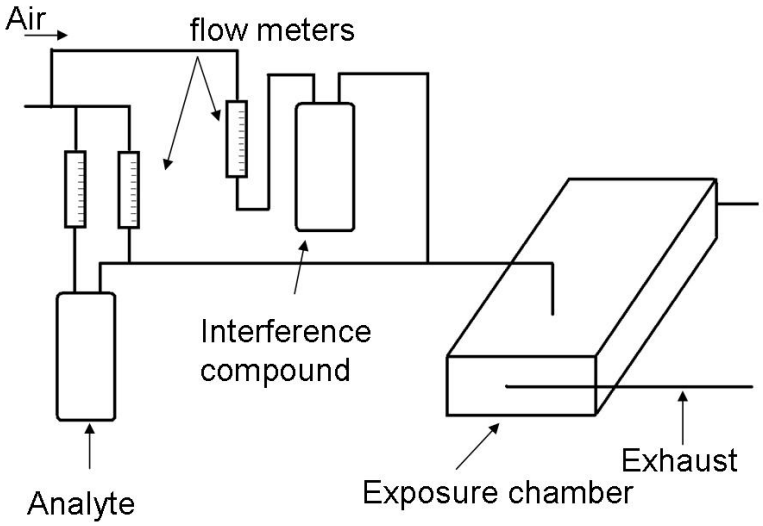

Figure 3. Two analyte exposure chamber

A concentration ladder was developed using HCl in order to determine the differences between the two concentrations of gas being bubbled through the chamber. Initially, a 100mL solution of NaOH in water with a pH of roughly 8 was made. A fresh sample of NaOH was used for each exposure. Four exposures were run, using a fresh sample of NaOH each time; one exposure of each concentration for a blank and for HCl. The HCl used was a freshly made diluted sample with a pH of 2. The concentrations were varied by adjusting the flow meters to 0.8 ft^3/hr:0.2 ft^3/hr for the lower concentration and 0.7ft^3/hr:0.3ft^3/hr for the higher concentration. The flow was bubbled into the NaOH solution for 15 minutes and the pH was taken before and after exposure on two pH meters.

Data:

Sample	Blank 1i	Blank 1f	Blank 2i	Blank 2f	HCl 1i	HCl 1f	HCl 2i	HCl 2f
meter 1	8.44	7.03	7.03	6.80	8.07	6.90	8.23	6.68
meter 2	8.2	7.1	7.1	7.06	7.72	7.09	7.93	6.87
Avg pH	8.32	7.07	7.07	6.93	7.90	7.00	8.08	6.78

Calculations:
HCl Conc 1:
$[M_i]=10^{-pH} = 10^{-7.9} = 1.26 \times 10^{-8}$ M
$[M_f]=10^{-pH} = 10^{-7.0} = 1.00 \times 10^{-7}$ M
$[M] = 1.00\times10^{-7}$ M - 1.26×10^{-8} M = 8.74×10^{-8} M
HCl Conc 1 (ppm): (8.74×10^{-8} M)(36.5g/mol)(1000mg/g)(10) = 0.032 ppm

HCl Conc 2:
$[M_i]=10^{-pH} = 10^{-8.08} = 8.32 \times 10^{-9}$ M
$[M_f]=10^{-pH} = 10^{-6.78} = 1.66 \times 10^{-7}$ M
$[M] = 1.66\times10^{-7}$ M – 8.32×10^{-9} M = 1.58×10^{-7} M
HCl Conc 2 (ppm): (1.58×10^{-7} M)(36.5g/mol)(1000mg/g)(10) = 0.058 ppm

Flow Rate for both analytes: $1ft^3$/hr
Flow Time for both analytes: 15 min

Volume of gas for both concentrations if assume 100% completion.
$(1ft^3/hr)(1728in^3/ft^3)(16.387cm^3/1in^3)(1mL/cm^3)(1L/1000mL)(1hr/60min)(15min)=7.08L$

Therefore, the ppm for gas of HCl at Conc 1 and at Conc 2 is:
M_{g1} = [(0.032ppm)(0.1L)]/7.08L = 4.52×10^{-4} ppm
M_{g2} = [(0.058ppm)(0.1L)]/7.08L = 8.19×10^{-4} ppm

Acid and base samples were analyzed with this method as well as a similar method involving neutralization of a solution injected into the gas sampling bag. The organic gas samples were injected into a Perkin Elmer GC-MS where the concentration was determined against a calibration curve for that compound. As each calibration curve required a large amount of work not all of these samples have been run, however it is possible to get a rough idea of concentration by comparing the size of each peak to other samples and the total ion count.

Library Development and Analysis

During the library development stage of this work we scanned 45 compounds at 2 concentrations with a number of repeats conducted on some of the analytes. For each of these scans we have 96 wells of data containing pre and post readings on 5 adsorption values along with fluorescence spectra from 4 illumination wavelengths. As many of these compounds were generic sensing compounds and the several of the compounds tested were similar in structure the response recorded for each compound returned a great

deal of data which had overlap with other analytes. A list of the analytes examined follows.

Acids: Hydrochloric Acid, Nitric Acid, Sulfuric Acid, Acetic Acid.
Bases: Ammonia, Household Bleach.
Organics: Toluene, Acetone, Ethanol, Methanol, Isopropyl Alcohol.
Pesticides: DEET, Malathion, Parathion, Ethion, Fenthion, Paraoxon.
Fuels: Diesel, Unleaded 85 Gasoline, Kerosene.
Toxic Organics: DMMP, DCP, Formaldehyde.
Combinations: DCP and Diesel, DCP and Unleaded 85 Gasoline, DCP and Kerosene

Algorithms were developed to track peak position and intensity as well as the change in adsorption values. Over the course of the project the search routines were fine tuned, however coding the data returned to accurately describe the response of the analyte proved quite problematic as we did not know what the response that we were looking for would look like, that is a peak shift characteristic of DCP or a shift in intensity from one wavelength to another. A numbered coding scheme was developed which gave an indication of the size and direction of the peak responses. To demonstrate the process a single wavelength of excitation was used which returned seven candidates for nerve gas detection. When the entire library was examined for the response of these seven compounds two more of the compounds were removed for returning too many false positives. However by comparing the remainder of the responses there are no other compounds which return an identical response. However using this single wavelength we are also not able to identify the nerve gas analog in the presence of an interference compound such as gasoline.

	A 4	A 10	D 5	D 11	E 1	E 7	E 2	E 8	E 3	E 9
DCP Con1.xls	541	541	541	541	541	541	541	541	541	541
DCP Con2.xls	341	341	431	341	531	541	541	311	422	412
DCP and Diesel x1.xl	341	240	340	340	541	541	341	340	441	541
DCP and Diesel x2.xl	341	340	431	341	431	441	431	333	441	441
DCP and Gas x1.xls	441	341	441	233	541	541	241	221	331	241
DCP and Gas x2.xls	241	342	441	441	541	541	341	342	341	321
DCP and Kerosine x1	212	233	341	341	542	521	241	241	232	231
Ethion Con1.xls	233	242	201	212	532	502	211	212	432	301
Ethion Con2.xls	542	542	341	241	541	541	542	542	541	341
Fenthion Con1.xls	311	201	321	341	531	511	211	211	311	421
Fenthion Con2.xls	231	231	321	301	541	501	421	211	322	301
H2SO4 Con1.xls	431	441	431	431	511	511	501	221	401	411
H2SO4 Con2.xls	331	442	402	321	502	531	431	331	422	311
H2SO4 Conc 2 Repea	331	231	240	441	541	521	441	211	311	502
Kerosene Con1.xls	231	231	240	321	522	511	441	331	401	402
Kerosene Con2.xls	541	541	212	341	542	542	212	232	541	541
Malathion Con1.xls	431	231	431	331	511	511	221	421	402	342
Malathion Con2.xls	541	541	342	242	532	542	541	541	322	342
NH3 Conc 2 Repeate	441	240	443	542	543	543	422	340	543	531
NH3 Conc 2 Repeate	240	240	542	542	521	533	332	242	543	531
Paraoxon Con1.xls	542	542	241	240	542	512	542	512	240	242
Paraoxon Con2.xls	231	241	331	311	521	511	231	541	421	431
Parathion Con1 repea	221	221	341	331	501	511	221	211	302	322
Parathion Con2.xls	511	511	112	111	231	431	511	501	201	123
Toluene Con1.xls	541	541	341	341	240	242	340	541	211	211
Unleaded 85 Con1.xls	541	321	342	442	542	542	541	541	402	431
Unleaded 85 Con2.xls	302	521	421	331	502	511	441	341	422	411

Figure 4. All of the DCP exposures and all of the other compounds which yielded a strong response to the 5 best candidates for 330 nm excitation in duplicate.

This same procedure can be conducted with the adsorption data where the 5 wavelengths tracked are examined and the best candidates for detecting DCP are picked, see Figure 5. For demonstration purposes the 450nm data is enough to shown that when we compare the signature of responses to the library of responses there are no samples that have an identical pattern, see figure 6. However much like the fluorescence data we are not able to detect our nerve gas analog when an interference compound is present, note that the samples in figure 7 containing DCP in addition to another molecule do not have similar patterns to that of DCP.

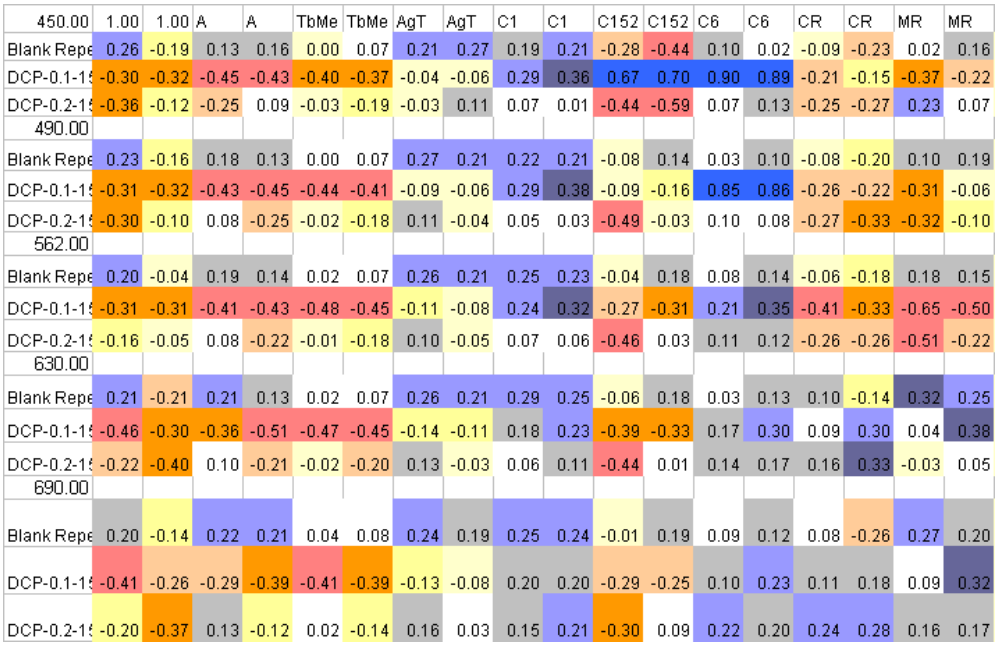

450.00	1.00	1.00	A	A	TbMe	TbMe	AgT	AgT	C1	C1	C152	C152	C6	C6	CR	CR	MR	MR
Blank Repe	0.26	-0.19	0.13	0.16	0.00	0.07	0.21	0.27	0.19	0.21	-0.28	-0.44	0.10	0.02	-0.09	-0.23	0.02	0.16
DCP-0.1-1	-0.30	-0.32	-0.45	-0.43	-0.40	-0.37	-0.04	-0.06	0.29	0.36	0.67	0.70	0.90	0.89	-0.21	-0.15	-0.37	-0.22
DCP-0.2-1	-0.36	-0.12	-0.25	0.09	-0.03	-0.19	-0.03	0.11	0.07	0.01	-0.44	-0.59	0.07	0.13	-0.25	-0.27	0.23	0.07
490.00																		
Blank Repe	0.23	-0.16	0.18	0.13	0.00	0.07	0.27	0.21	0.22	0.21	-0.08	0.14	0.03	0.10	-0.08	-0.20	0.10	0.19
DCP-0.1-1	-0.31	-0.32	-0.43	-0.45	-0.44	-0.41	-0.09	-0.06	0.29	0.38	-0.09	-0.16	0.85	0.86	-0.26	-0.22	-0.31	-0.06
DCP-0.2-1	-0.30	-0.10	0.08	-0.25	-0.02	-0.18	0.11	-0.04	0.05	0.03	-0.49	-0.03	0.10	0.08	-0.27	-0.33	-0.32	-0.10
562.00																		
Blank Repe	0.20	-0.04	0.19	0.14	0.02	0.07	0.26	0.21	0.25	0.23	-0.04	0.18	0.08	0.14	-0.06	-0.18	0.18	0.15
DCP-0.1-1	-0.31	-0.31	-0.41	-0.43	-0.48	-0.45	-0.11	-0.08	0.24	0.32	-0.27	-0.31	0.21	0.35	-0.41	-0.33	-0.65	-0.50
DCP-0.2-1	-0.16	-0.05	0.08	-0.22	-0.01	-0.18	0.10	-0.05	0.07	0.06	-0.46	0.03	0.11	0.12	-0.26	-0.26	-0.51	-0.22
630.00																		
Blank Repe	0.21	-0.21	0.21	0.13	0.02	0.07	0.26	0.21	0.29	0.25	-0.06	0.18	0.03	0.13	0.10	-0.14	0.32	0.25
DCP-0.1-1	-0.46	-0.30	-0.36	-0.51	-0.47	-0.45	-0.14	-0.11	0.18	0.23	-0.39	-0.33	0.17	0.30	0.09	0.30	0.04	0.38
DCP-0.2-1	-0.22	-0.40	0.10	-0.21	-0.02	-0.20	0.13	-0.03	0.06	0.11	-0.44	0.01	0.14	0.17	0.16	0.33	-0.03	0.05
690.00																		
Blank Repe	0.20	-0.14	0.22	0.21	0.04	0.08	0.24	0.19	0.25	0.24	-0.01	0.19	0.09	0.12	0.08	-0.26	0.27	0.20
DCP-0.1-1	-0.41	-0.26	-0.29	-0.39	-0.41	-0.39	-0.13	-0.08	0.20	0.20	-0.29	-0.25	0.10	0.23	0.11	0.18	0.09	0.32
DCP-0.2-1	-0.20	-0.37	0.13	-0.12	0.02	-0.14	0.16	0.03	0.15	0.21	-0.30	0.09	0.22	0.20	0.24	0.28	0.16	0.17

Figure 5 . The visual adsorption response to DCP at all 5 wavelengths based on the best responses observed.

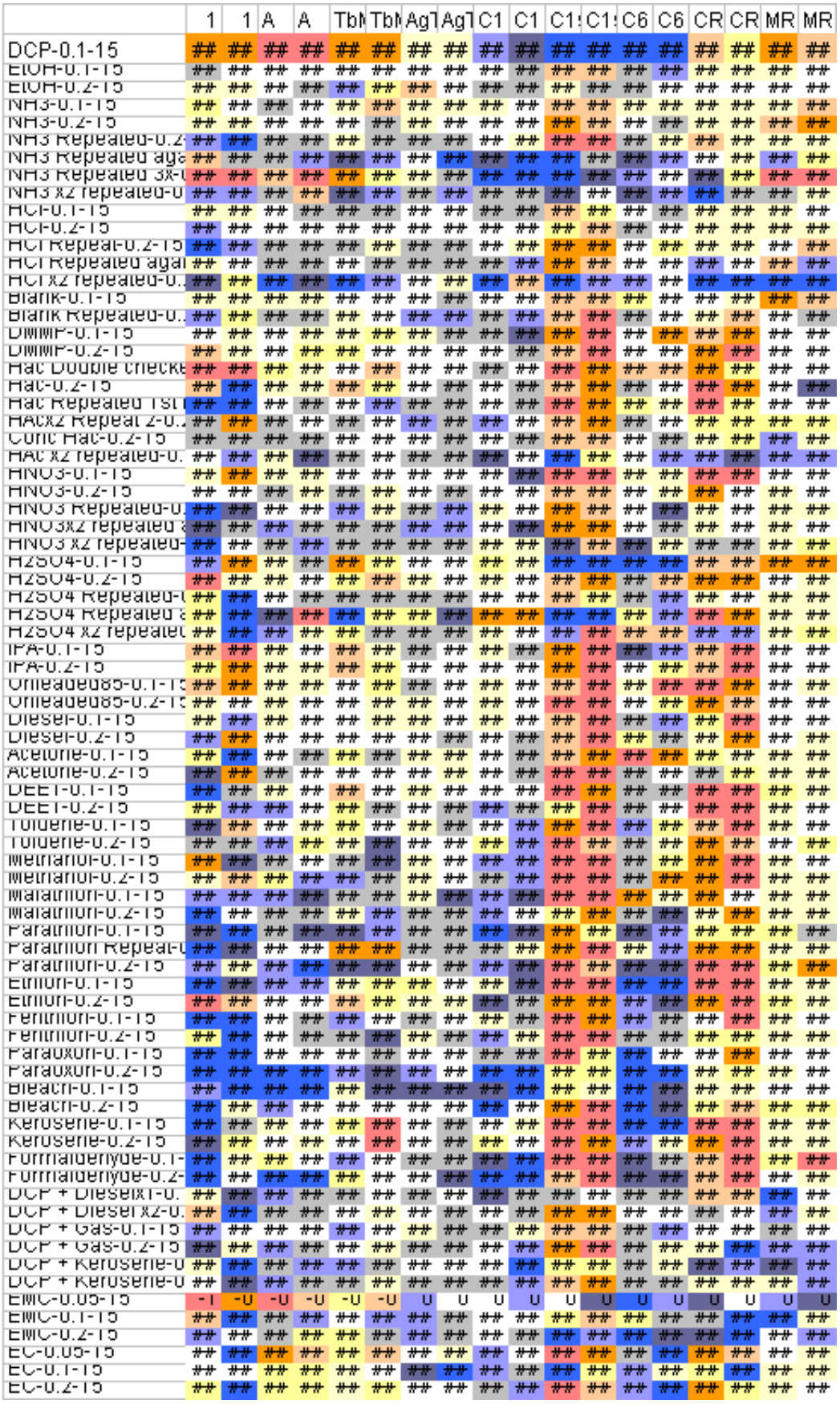

Figure 6. Response of all compounds tested to the 5 best candidate sensing molecules

	1.0	1.0	A	A	TbM	TbM	C1	C1	C15	C15	C6	C6	MR	MR
DCP-0.1-15	-0.3	-0.3	-0.5	-0.4	-0.4	-0.4	0.3	0.4	0.7	0.7	0.9	0.9	-0.4	-0.2
NH3 Repeated again-0.2-15	-0.3	0.1	0.2	0.3	0.3	0.2	0.4	0.6	0.6	0.2	0.3	0.3	0.2	-0.1
NH3 Repeated 3x-0.2-15	-0.6	-0.8	-0.2	-0.5	-0.4	-0.2	0.5	0.8	0.7	0.4	0.2	0.1	-0.9	-0.8
NH3 x2 repeated-0.2-15	0.3	0.2	0.2	-0.3	0.3	0.3	0.2	0.2	0.3	0.0	0.3	0.3	0.2	-0.1
H2SO4-0.1-15	0.2	-0.3	0.0	0.1	-0.4	-0.1	-0.1	-0.1	0.7	0.8	0.8	0.8	-0.3	-0.4
H2SO4 Repeated again-0.2	-0.1	0.8	0.3	-0.6	0.6	-0.2	-0.3	-0.3	0.9	0.4	-0.2	0.3	-0.1	0.0
H2SO4 x2 repeated-0.2-15	-0.1	0.6	0.2	0.0	-0.1	0.1	-0.1	0.1	0.3	-0.4	-0.2	-0.3	0.0	-0.1
IPA-0.1-15	-0.2	-0.4	0.0	0.0	-0.2	0.0	0.0	0.1	-0.3	-0.5	0.3	0.3	0.0	0.0
IPA-0.2-15	-0.2	-0.3	0.0	-0.1	-0.2	-0.1	0.0	0.0	-0.3	-0.5	0.0	-0.2	0.0	0.0
Malathion-0.1-15	0.3	0.3	0.2	0.3	0.2	0.2	0.3	0.3	-0.5	-0.5	-0.3	0.0	0.0	-0.1
Malathion-0.2-15	0.5	0.0	0.1	0.2	-0.1	0.2	0.2	0.1	-0.2	-0.3	0.1	0.3	-0.1	0.0
Parathion-0.1-15	0.3	0.5	0.2	0.3	0.3	0.3	0.5	0.4	-0.4	-0.2	0.3	0.3	-0.1	0.2
Parathion Repeat-0.1-15	0.6	0.4	0.1	0.0	-0.3	-0.4	0.1	0.0	-0.4	-0.5	-0.1	0.3	0.0	0.0
Parathion-0.2-15	0.2	0.0	0.2	0.6	0.3	0.3	0.3	0.3	-0.4	-0.3	0.4	0.4	-0.1	-0.3
Ethion-0.1-15	0.6	0.4	0.3	0.3	0.0	-0.2	0.0	0.3	-0.6	-0.5	0.5	0.6	-0.1	0.0
Ethion-0.2-15	-0.6	-0.2	0.1	0.0	-0.3	-0.2	0.4	0.1	-0.4	-0.4	0.3	0.3	-0.1	-0.1
Fenthion-0.1-15	0.5	0.5	0.0	0.1	0.3	0.1	0.0	0.1	-0.5	-0.3	0.2	0.2	-0.1	0.0
Fenthion-0.2-15	-0.1	0.6	0.1	0.1	0.2	0.3	0.2	0.0	-0.4	-0.4	0.2	0.2	0.0	-0.1
Paraoxon-0.1-15	0.4	0.4	0.1	0.1	0.0	0.1	0.1	0.1	-0.4	-0.1	0.5	0.1	0.0	0.0
Paraoxon-0.2-15	0.6	0.6	0.6	0.4	0.3	0.3	0.7	0.6	-0.2	-0.2	0.7	0.6	-0.1	0.0
Bleach-0.1-15	0.2	0.7	0.6	0.5	0.0	0.3	0.3	0.5	-0.1	0.0	0.6	0.4	0.0	0.1
Bleach-0.2-15	0.6	0.0	0.2	0.0	0.1	0.1	0.5	0.1	-0.4	-0.4	0.4	0.4	-0.2	-0.1
Formaldehyde-0.1-15	0.5	-0.1	-0.2	0.0	0.2	0.1	0.3	0.4	-0.5	-0.5	0.3	0.1	-0.2	-0.5
Formaldehyde-0.2-15	0.7	0.1	0.4	0.5	-0.2	0.1	0.5	0.5	-0.3	-0.4	0.3	0.4	0.0	0.0
DCP + Dieselx1-0.1-15	0.0	0.4	0.2	0.1	0.1	0.1	0.4	0.1	0.2	0.1	0.2	0.2	0.5	0.0
DCP + Diesel x2-0.2-15	-0.3	0.6	0.2	0.2	0.1	0.0	0.1	0.2	-0.4	-0.4	0.0	0.0	0.2	-0.1
DCP + Gas-0.1-15	0.2	0.1	0.0	0.1	0.3	0.0	0.1	0.0	-0.3	-0.3	0.2	0.2	0.1	0.1
DCP + Gas-0.2-15	0.4	-0.1	0.2	0.1	0.0	0.0	0.0	0.3	-0.3	-0.4	0.1	-0.1	0.2	0.3
EMC-0.05-15	-0.6	-0.4	-0.4	-0.3	-0.1	-0.2	0.1	0.2	0.1	0.4	0.5	0.3	0.3	0.4
EMC-0.1-15	-0.2	0.7	0.1	0.2	0.0	0.2	0.0	0.0	-0.2	-0.3	-0.1	0.2	0.7	-0.1
EMC-0.2-15	0.3	0.0	0.1	-0.2	-0.2	0.1	0.0	0.2	0.7	0.2	0.5	0.4	0.0	0.3
EC-0.05-15	0.0	0.6	-0.3	-0.2	-0.1	-0.2	0.2	0.0	-0.5	-0.4	0.1	0.4	0.0	0.0

Figure 7. Response of all compounds giving a false positive. Using a single dye no compound returned no false positives, however when multiple dyes are combined it is possible to create a unique finger print of the tested compounds. It should be noted that although we can eliminate false positives in this manner we can not weed out the nerve gas analog in the presence of an interference compound.

As a final examination of the data all of the fluorescent and adsorption data was scanned visually and given a coded response based on the overall response, the adsorption response and the fluorescent response at each wavelength. This method was much slower than the automated search routines, however it did lend itself to qualitative judgments based on intensity shifts as well as allowed for corrections to be made for incomplete or damaged data. Using this method we were able to identify one of the Western Michigan Compounds, compound 3, which showed a drop in intensity at all 4 excitation wavelengths which was only present with DCP, the high concentration samples of DMMP and ethion, acetic acid, and all of the samples of DCP with an interference compound. As DMMP, ethion and acetic acid were all easily distinguishable using other compounds it appears that we have found a prime candidate for detecting DCP in the presence of fuels. The choice of the other sensing compounds which would fill out the suite on the sensor would be dictated by the other compounds that would be desirable to detect.

Prototype Development

In order to produce an inexpensive sensing device we believe it is necessary to co-opt other technology which is already being produced on a large scale. The primary focus of the research at Altair has been to develop or discover a dye or set of dyes which exhibit either a fluorescence or absorption change indicative of a nerve gas or toxic industrial chemical. Both of these changes require a device which can produce an electric response to an optical change. Charge Coupled Device (CCD) arrays are very common commercially available devices which are produced in large scale and therefore very inexpensive, providing a device with spatial sensitivity as well as the required optical sensitivity needed for the measurement.

Receiving a signal is one aspect of the sensing device, however it is also important to provide light at various wavelengths to better record the optical response in both absorption and fluorescence. There are multiple companies who are now producing chips which have been built to incorporate multiple LEDs of various wavelengths. These devices are ideal as they provide a fairly narrow band light source, are low energy consumptive, durable and inexpensive. In the last several years the wavelengths which are available for these devices has also greatly increased making incorporation of these devices much easier. For the work that we are performing here we have chosen an LED chip set with 9 addressable LEDS or differing wavelengths, ranging from 380nm to 800 nm

To use the full potential of the CCD chip the pixels have to be assigned a color value. In commercial CCD arrays there is a set of color filters which fits over the chip and assigns a pixel to either red green or blue. However these filters are not appropriate for or device and it is more useful to build our own filter array to fit over the camera chip. The choice or filter material has a great deal to do with the final function of the device and the need for wavelength sensitivity. The lowest cost solution that we have found is the use of gel filter sheets. These sheets are used in the lighting industry to tailor the look of light by cutting out certain wavelengths of light, because of this a wide variety of filters have been developed, and many of the associated calendar life problem shave been addressed to allow for a filter which exhibits very little photo bleaching and shifts in absorption characteristics over the life time of the filter.

Another possibility that could fulfill the filtering requirement of the device would be the use of dichroic filters. These filters use interference to eliminate unwanted wavelengths and can be tailored to have a very narrow band pass. Because of the higher control over bandpass these filters would be better able to monitor a small wavelength shift. Unlike the gel filters these filters are composed of multiple layers of inorganic coatings deposited using circuit printing techniques. The processing used in these devices allows the filters to be patterned during the production with spatial resolution in line with that of the individual pixels of the CCD array. The drawback of these devices is that a large initial investment is required to design the coating process that yields the required bandpasses. Once the device is being manufactured this is much less of a

problem as each printing yields a very large number of filter arrays, however for the prototype development the incorporation of this technology would be prohibitively expensive.

As a group we have recognized that air flow in the sensing device can have a huge effect on whether or not the device functions at the level shown in the laboratory. While optimization of our prototype would require extensive study of the air flow in the apparatus, we believe it is in the best interest of this project to refrain from the testing necessary and optimize the air flow. Instead we have incorporated an SKC gas sampling unit into the prototype to pull an air stream across the surface of the sensing array. This device is the largest single unit of the prototype, however a large portion of this volume is devoted to a rechargeable battery for the device and the necessary case to protect the inner workings. In the finished device the power source would be incorporated and the chassis would be designed to incorporate all of the pieces of the sensor.

By placing the light source directly in line with the CCD chip and placing the sensing array as close to the CCD as possible the spread of fluorescent light from the sensing compound can be minimized. This means it is easier to track which compound responds to which, and has the added benefit that the highest intensity of the fluorescent compound is also seen.

As previously mentioned the sensor can be designed to work in both adsorption mode and also in fluorescence mode. In adsorption mode a set of filters is chosen to allow a large area of the sensor to act as a pixel for a given wavelength of light. Note that in the following images we have been using a color CCD chip, which has introduced a number of problems. As this chip is a color recording chip there is an integrated white balance algorithm which adjusts all of the pixel values so that the “whitest” pixel is white. This algorithm can seriously shift the color response when the chip is illuminated with a monochromatic source as is the case here. This can clearly be seen in the “a” image where the blue illumination has produced a very red heavy response in many of the pixels. Also since the chip is reading color the spatial resolution is not as great as we could have achieved with a monochromatic CCD array, however for a proof of concept there is enough control with these chips to achieve the desired result. For demonstration purposes the filters have been placed parallel to each other and covering the entire CCD array and the sensing complexes would be placed perpendicular in a similar configuration. In practice this would be an array spread over the surface to avoid a large signal bleeding into an adjacent area and giving a false signal. The center filter in the following set of images demonstrates that we can use a filter to only allow light of a given wavelength to illuminate area, as can be seen with the 405 nm illumination.

a) 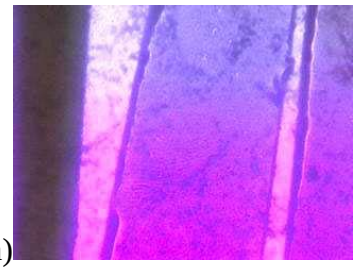 b) 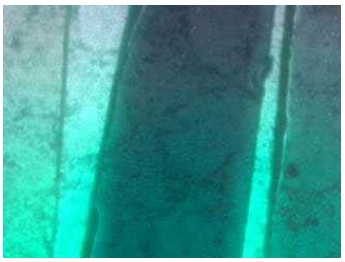 c) 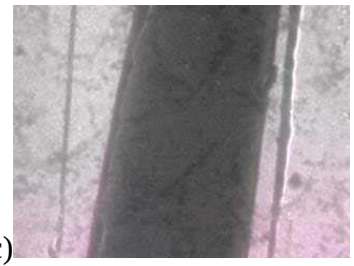

Figure 8. The above images demonstrate the sensor working in adsorption mode with the same image illuminated by different wavelengths of light. In “a” the area is illuminated with 405 nm light and is blocked by the leftmost filter. In “b” the illumination wavelength is 495 which is blocked by the center filter and partially by the right hand filter, while the 630nm illumination of “c” is only blocked by the center filter.

The following figure shows the sensor operating in a fluorescence mode. On the right portion of the image the fluorescent dye is coated on to a mylar sheet. There is a filter dye which covers the entire CCD array and blocks radiation below 450 nm in wavelength. When a 530 nm illumination is used the fluorescent dye blocks a larger portion of the light in that section of the detector and we see less intensity. However when the illumination is shifted to 405nm the dye coated array now emits at a much higher wavelength and we see the dye coated area is now displaying a much larger intensity. These two figures also demonstrate the main drawback when using the device in fluorescence; the incoming light is direct so that the light that interacts with the dye is then moving on to interact with the pixel directly below that point and maintains a fairly high resolution. However when the device is used in fluorescence mode the light which is absorbed is emitted in randomly in every direction, because of this there is bleed over from the dye coated area to the remainder of the slide. This leakage of light can be mitigated by greatly reducing the distance between the dye and the CCD array or placing a larger spatial separation between pixels.

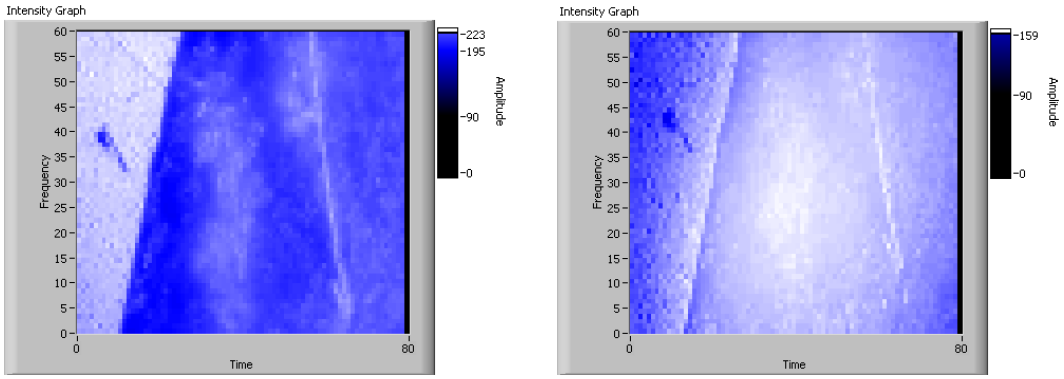

Figure 9. The left image is of the dye coated slide illuminate with 530 nm light, while the right side image is the same slide illuminated with 405 nm light

To demonstrate the proof of concept we coated a mylar slide with a thin film of cresol red, a pH sensitive dye. After initial measurements were recorded on the sample the plate was exposed to an acid vapor stream as well as a base vapor stream. As can be seen in the following table there was a clear distinction between the two exposures that

were in line with both the full spectra visual data and the resolution and sensitivity of the system.

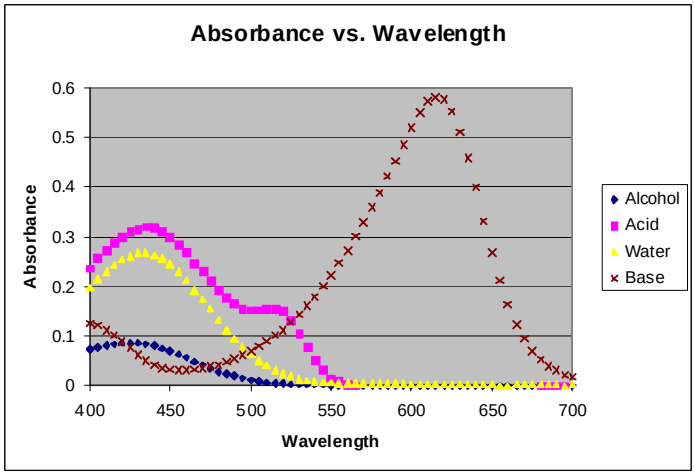

Figure 10. Visual adsorption data for cresol red at various in neutral, acidic and basic conditions. Response of sensor to acidic and basic conditions at various wavelengths

Wave-length	Base exposure	Acid exposure
405	-18%	29%
470	-6%	-38%
595	-24%	15%
650	-6%	35%

Table 1. Response of cresol red on mylar to acidic and basic conditions at four illumination wavelengths. There is a clear demonstration of the ability of this sensor to distinguish between responses which fall in line with the UV-Vis spectra.

FINAL REPORT

Contract No. W911NF-09-C-0135

Part II. Altairnano Lithium Ion Nano-scaled Titanate Oxide Cell and Module Abuse Test Report

Authors: Michael Reed and Dave Miller

Altairnano Lithium-Ion Nano-Scaled Titanate Oxide Cell and Module Abuse Test Report

Crane Document Number: GDD GXS 11-053 (Preliminary Report)
Issue Date: 05/3/2011

Naval Surface Warfare Center, Crane Division
Energy Power & Interconnect Technologies Division
Code GXSM

Distribution Statement A:	Approved for public release; distribution is unlimited. Requests for this document shall be referred to NAVSEA CRANE.
Destruction Notice:	For classified documents, follow the procedures in DOD 5200.22m, Industrial Security Manual, Section 11-19 or DOD 5200.1-R, Information Security Program Regulation, Chapter IX. For unclassified, limited documents, destroy by any method that will prevent disclosure of contents or reconstruction of the document.

Review and Approval Sheet

Document Title	**Altairnano Lithium-Ion Nano-Scaled Titanate Oxide Cell and Module Abuse Test Report**		
Part Number(s)	Altairnano Lithium-Ion Nano Titanate Cells: 010-052-0001 Altairnano Lithium-Ion Nano Titanate Modules: Mark 1		
Document Number	GDD GXS 11-053		
	Name	**Signature**	**Date**
Prepared By:	Michael Reed		
Reviewed By:	Lilia Haro		
Test Engineer:	Michael Reed		
GXSM Branch Manger	Dave Miller		

Table of Contents

List of Figures

List of Tables

1 Introduction

1.1 Task Overview

Crane Division, Naval Surface Warfare Center (NSWC Crane) Test & Evaluation Branch (Code GXSM) was tasked by Altairnano to perform safety abuse testing on Lithium Nano-Scale Titanate Oxide Cells and Modules. Cell testing included overcharge testing, cell overheating, the investigation of thermal propagation between cells, and vent gas analysis of overcharged/overheated cells. Module testing included thermal propagation between cells, overcharge testing, overheat testing (via flame and/or heat tape), and determining the effectiveness of carbon dioxide, water, and FM200 in suppressing a Mark I module fire. The tests performed are improved or modified versions of test called out in NAVSEA TM-S9310 which are tests designed to provoke worst-case scenario responses from the cells/modules for preliminary assessment purposes and for identifying battery vulnerabilities.

1.2 Test Item Background

Typical Li-Ion batteries are inherently unstable due to the undesirable reactions between the graphite electrodes and the electrolyte which can ultimately cause the battery to reach thermal runaway and catch fire. This instability has lead to complex control systems that monitor and control individual cell voltages, charges, and temperatures. Such systems have proven adequate for small battery applications, such as cell phones and laptops, yet pose too much risk as larger power systems. Alternative electrode and electrolyte materials are extensively being researched to solve the underlying issues preventing lithium ion batteries from being used in large scale applications. One possible candidate actively being researched by Altairnano as a replacement to the intrinsically problematic carbon anode material in lithium ion batteries is lithium titanate ($Li_4Ti_5O_{12}$).

Lithium titanate has shown preferential qualities as an intercalation electrode material. It's lower than typical, but steady, operating voltage of 1.5 V versus the Li^+/Li couple decreases the risk of plating metallic lithium and thus thermal runaway events. The nano-sized particles allow for excellent rate capability while displaying minimal expansion and contraction fatigue during intercalation and de-intercalation reactions. Additionally, unlike graphite electrodes, lithium titanate does not form performance limiting SEI layers. All these unique properties suggest that lithium titanate as an electrode material can offer high performance and increased cycle life at a lower risk.

1.3 Test Item Description

Altairnano supplied NSWC Crane with thirty 11 Ahr Cells (Altairnano part number 010-052-0001) and four Mark I Modules. The specifications sheet for these cells can be found in Appendix B: Altairnano Cell Charging Profiles. The following table gives a description of the cell chemistries and configurations.

ALTAIRNANO 11 AMP HOUR CELL SPECIFICATION DATA	
Operating Temperature Range	-40°C to +55°C
Nominal Voltage	2.3 V
Nominal Capacity	11 Ah
Recommended Charge/Discharge Current	10 A
Recommended Fast Charge	66A (110A max)
Recommended Fast Discharge	110A
Typical Power	400 W and 1100 W/kg
Recommended Cut Off Voltage (-40°C to +30°C)	1.5 V
Recommended Cut Off Voltage (+30°C to +55°C)	2.0 V
Recommended Charge Cut Off (-40°C to +20°C)	2.8 V

Table 1: Altairnano Lithium Nano-Titanate Cell Specifications

1.4 Test Outline

Figure 1, page 4, categorizes the cell tests performed according to the type of test and the type of data obtained. Due to the complexity of some of the tests, the securement of funding, and due to the scheduling of test chambers, testing occurred over several months.

AltairNano Li-Ion Titanate Cell Test Overview

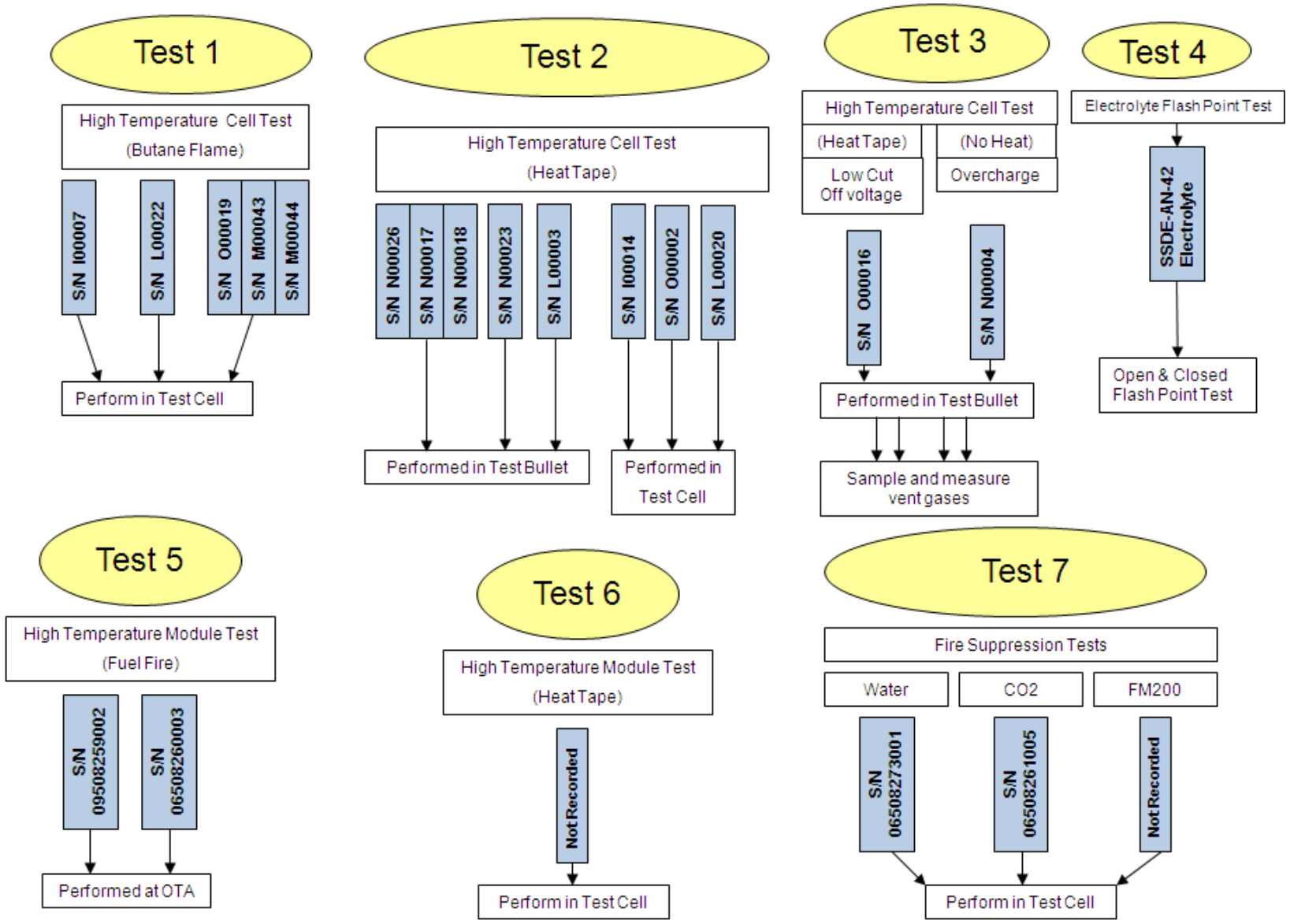

Figure 1: Altairnano Cell/Module Test Outline

1.5 Pre-Test Setup (Cell and Module Charging Procedure)

All cells were charged according to the following procedure with the exceptions of S/N O00016 and N00004. After placing the cells under a 217 kg compressive force, by means of bolting them between two aluminum plates, the cells were connected to a data acquisition system and a power supply. With the power supply set to a constant current mode, the cells were charged at 0.9 C (~10 Amps) until their final voltages reached 2.8 Volts. Figure 42, Appendix B: Altairnano Cell Charging Profiles, shows the charging profile for each cell. As can be seen on the figure, two of the charging profiles were set at a constant 30 Amps which was necessary for their 3 cell configurations with all 3 cells being simultaneously charged (~10 Amps per cell).

Cell's S/N O00016 and N00004 were prepared between two aluminum plates as stated for the previous cells; however, as required for Test 3, S/N O00016 was charged to 1.84 volts, the minimum recommended voltage at temperatures between 35 - 45°C, and used for the low cut off voltage overheat test. Since S/N N0004 would undergo charging during testing it was not charged prior to its use in Test 3 (Overcharge Test).

Prior to testing, all Altairnano Mark I modules were fully charged using the following procedure: The modules were charged at a current rate of 300 amps, removing the charging current when any of the cell voltages reached 2.8 volts. After removing the charging current the voltage was allowed time to stabilize and charging continued at a lower current rate of 100 amps until any of the cell voltages, again, read 2.8 Volts.

2 Test 1-Exposure to a High Thermal Flux (Butane Flame)

2.1 Introduction

Three tests were performed within a test chamber to determine the effects of a high thermal flux onto the side of a fully charged cell. The first two tests were single cells subjected to the butane flame. The third test consisted of three cells configured in series under compression with one of the cell's ends being subjected to the butane flame. Figure 2 depicts the configuration for which all three tests were setup.

2.2 Test Method

Prior to the remote activation of the butane Bunsen burner, the data acquisition system was set to record the cell voltages and thermocouples. The thermocouples, approximately 4-5 located around the periphery of both sides of the aluminum plates and attached with fiberglass tape, were present to monitor the maximum plate temperatures. The butane fuel supplied to the Bunsen burner was remotely disconnected after observing a drop in Cell voltage. In the case of the three cells configured in series, the fuel was turned off after the bottom cell's voltage (i.e. the cell closest to the flame) dropped to zero. All three tests were recorded via a video camera internal to the test chamber and are available for review.

Figure 2: Li-Ion Nano-Titante Cell Flame Test Setup (S/N I00007)

2.3 Cell Test #1: Results and Discussion

The temperature and voltage profile plotted versus time for cell S/N L00022 can be found in Figure 3. From the resulting curves it appears that with a high heat flux the battery reached a critical failure temperature (253°C) after which the battery vented, apparently through forced holes in the cell Mylar, Figure 4.

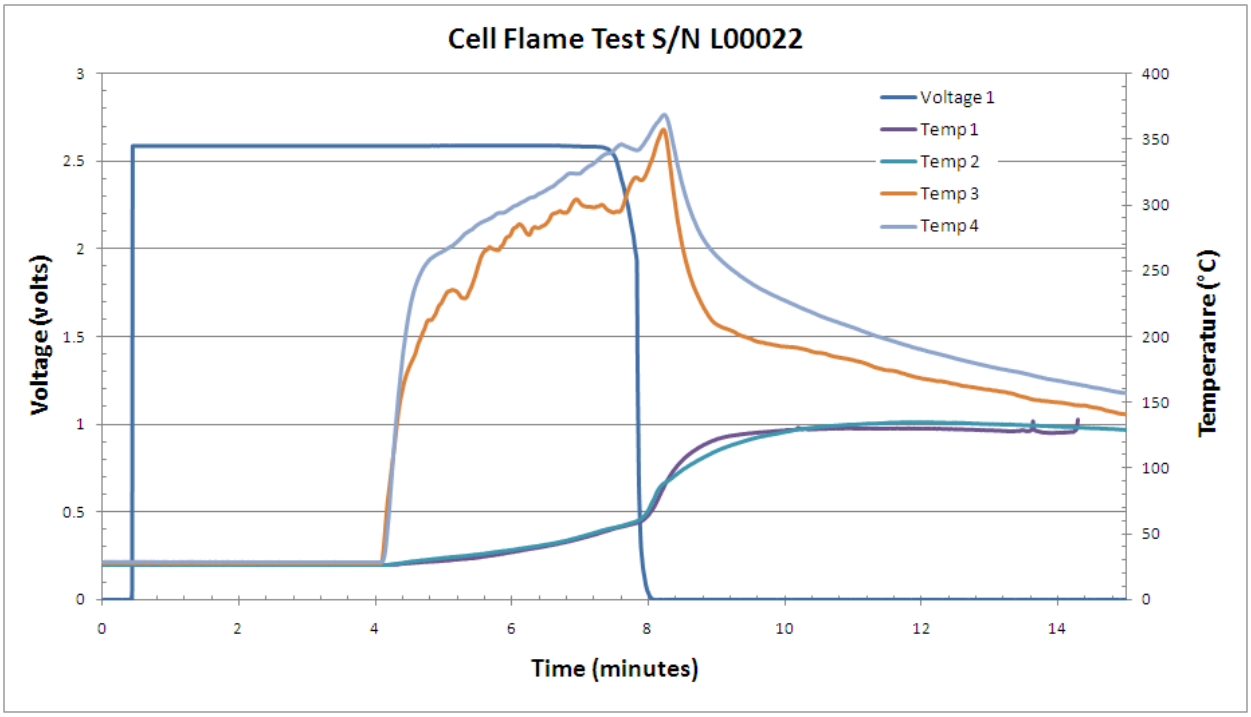

Figure 3: Cell S/N L00022 Flame Test Data

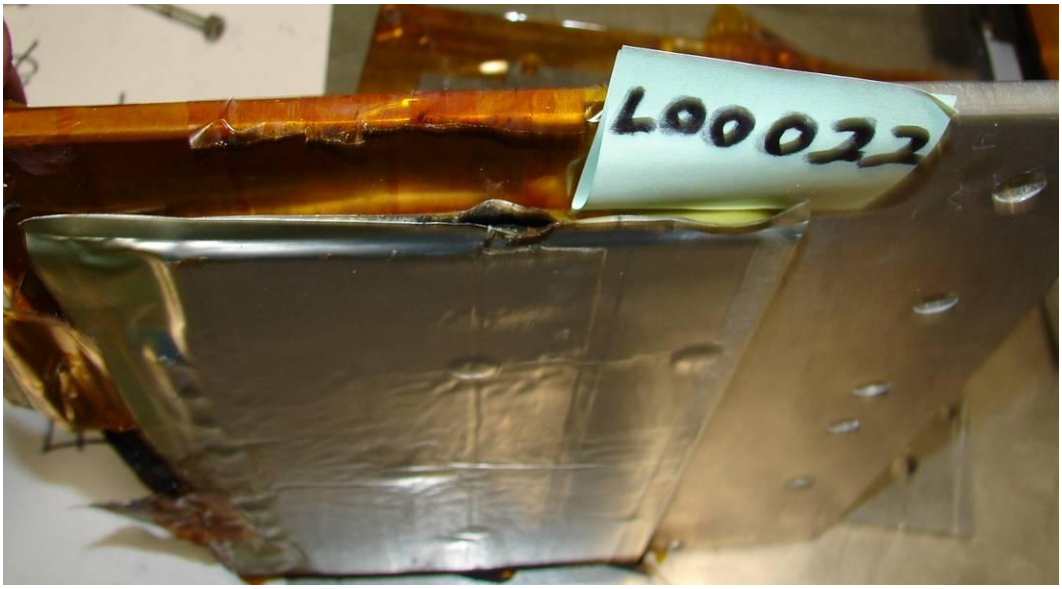

Figure 4: Li-Ion Nano-Titanate Cell Flame Test Cell Damage

As can be seen on the video screen shots, Figure 5 & Figure 6, a majority of the vaporized electrolyte exited the battery through the cell near the voltage tabs. After ~50 seconds of exposure to the Bunsen burner the cell vented electrolyte which quickly caught fire, Figure 5. At 1.57 minutes, the cell's venting process increased substantially, likely due to the majority of the electrolyte within the cell reaching its boiling point, resulting in large flames extending out of the front and side of the cell, Figure 6.

Figure 5: S/N L00022 Flame Test, Initial Cell Tab Flames

Figure 6: S/N L00022 Flame Test, Cell Venting

Figure 3 shows a constant rise in the bottom plate temperature (Temp 3 & 4) from 4 minutes to 8 minutes due to the constant heat provided by the Bunsen burner. The top plate temperature (Temp 1 & 2) rouse following the violent vent due to the increased flames around and beneath the top plate and from the exothermic reaction caused when the cell shorted.

2.4 Cell Test #2: Results and Discussion

For verification purposes, Cell S/N I00007 was subjected to the same test as described in Section 2.3. The test setup used is shown in Figure 7. The cell test data, Figure 8, reveals a similar curve as that obtained for Cell S/N L00022. An additional temperature probe (#5) was added to obtain the flame temperature directly above the Bunsen burner and was found to have a maximum recorded temperature of ~800°C (the limit of the probe). The video of the test revealed the same events as that previously stated for S/N L00022, Figure 9. Disassembly of the remains of S/N I00007, Figure 10 (left), revealed the large electrolyte vapor exit hole between the cell voltage tabs. The black circular

mark shown in Figure 10 (left) can be explained by observing the circular hole within the bottom aluminum compression plate, Figure 10 (right), which allowed for direct contact of the flame to the bottom cell.

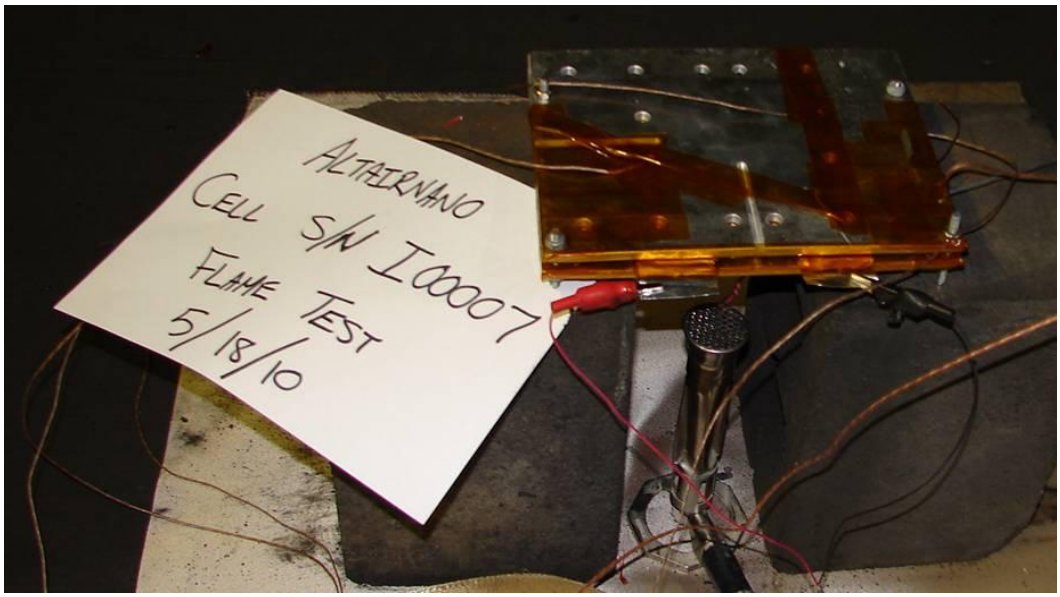

Figure 7: Altairnano Li-Ion Nano-Titanate Cell Flame Test Setup (S/N I00007).

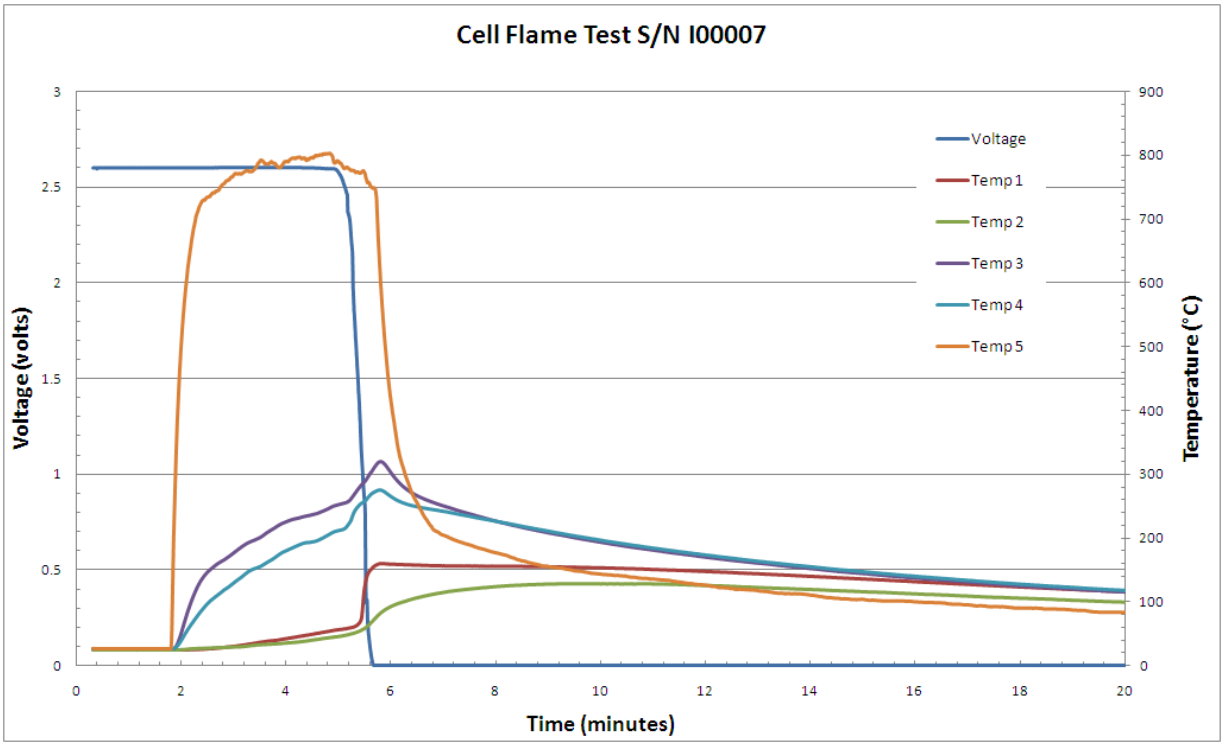

Figure 8: Cell S/N I00007 Flame Test Data.

Figure 9: Cell I00007 Flame Test Video Screen Captures.

Figure 10: Flame Test - Cell S/N I00007 After Test Photos

2.5 Cell Test #3: Results and Discussion

To investigate the heat propagation through adjacent cells, Cell S/Ns O00019, M00043, and M00044 were compressed between aluminum plates in a series configuration and subjected to the same test as the previous two cell described in Section 2.3 & 2.4, Figure 11.

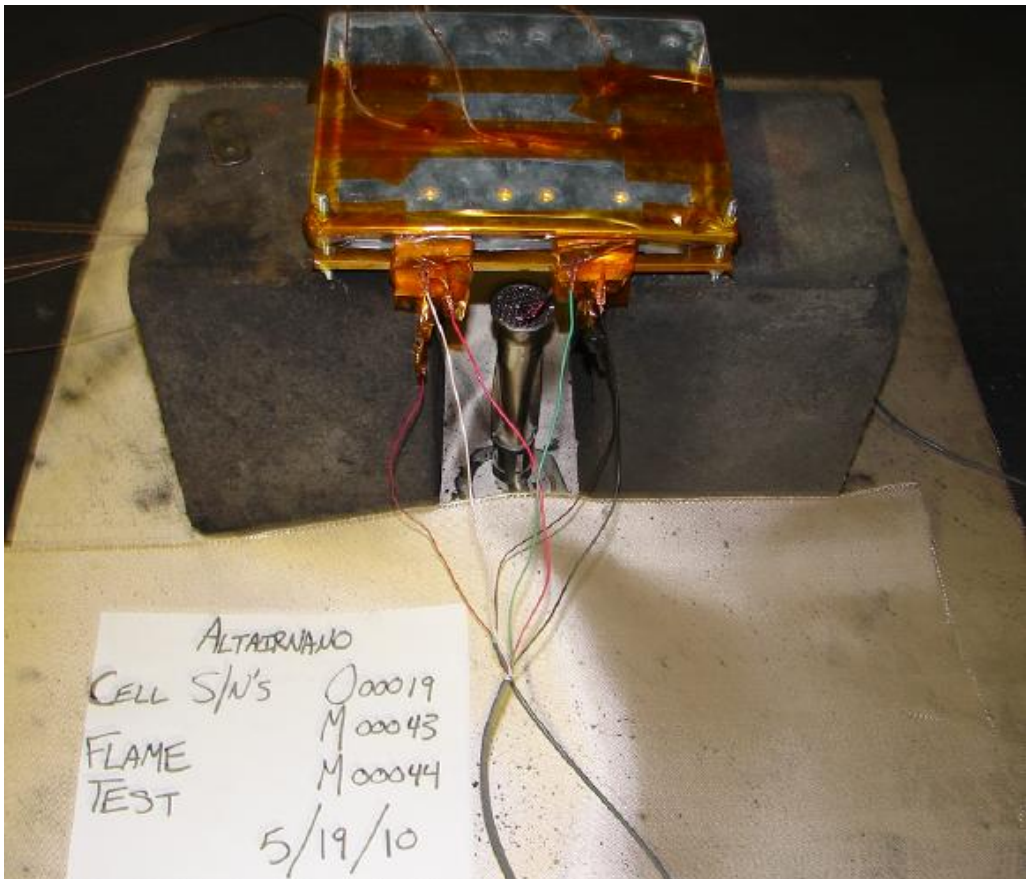

Figure 11: Li-Ion Nano-Titanate Cell Flame Test Setup (S/N O00019, M00043, M00044)

Comparing a plot of the thermocouple and voltage responses, Figure 12, to screen captures of the test video, Figure 13, the following observations can be made. Cell 1, which was closest cell to the Bunsen burner, caught fire after being subjected to 20 seconds of heat provided by the burner. After 02:12 Cell 1 violently vented and its gaseous electrolyte caught fire. Cell 1's fire quickly burned out and at 05:36 Cell 2 vented electrolyte and caught fire. The last cell vented and caught fire at 06:31. Interestingly, Cell 1's voltage held for ~ 60 seconds following its venting whereas the Cell 2 & 3 simultaneously lost their voltages when Cell 2 violently vented. It is likely that the voltage lines of both cells were damaged during Cell 2's venting thus causing it to read erratic values before dropping to zero. Although the heat from the Bunsen burner was kept on until the voltage of Cell 1 dropped to zero (~04:30 on Figure 12), the heat from the bottom aluminum plate and the heat generated from Cell 1 venting, propagated to Cell 2 causing it to vent. This process continued, acting as a chain reaction, and 55 seconds after Cell 2 vented Cell 3 vented.

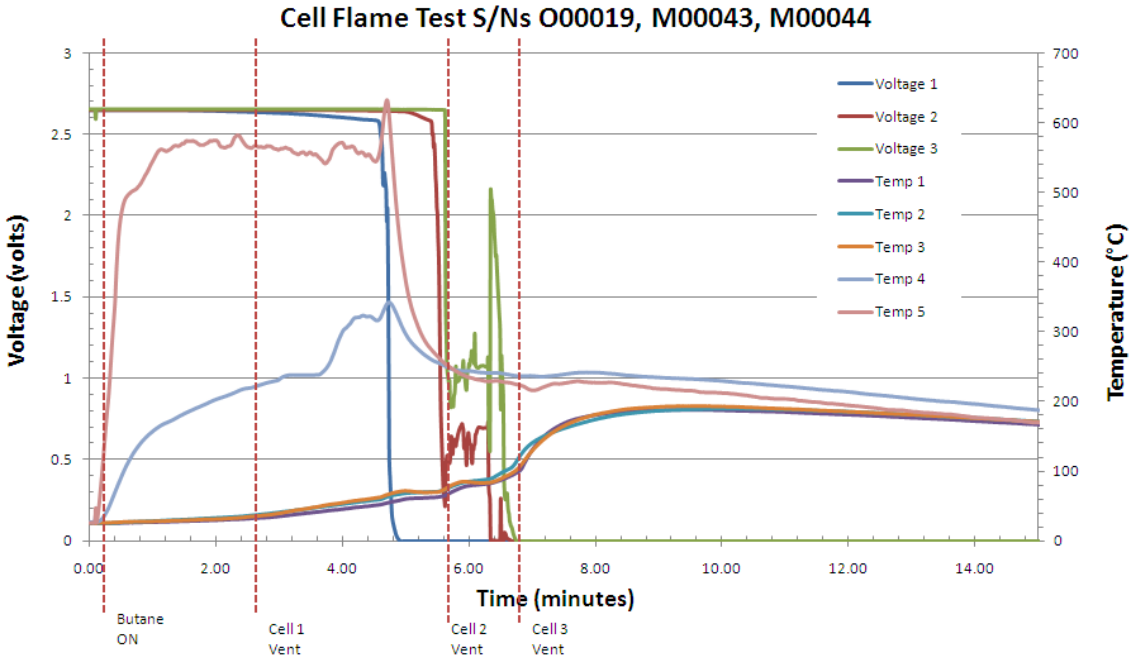

Figure 12: Altairnano Li-Ion Nano-Titanate Cell Flame Test (S/N O00019, M00043, M00044)

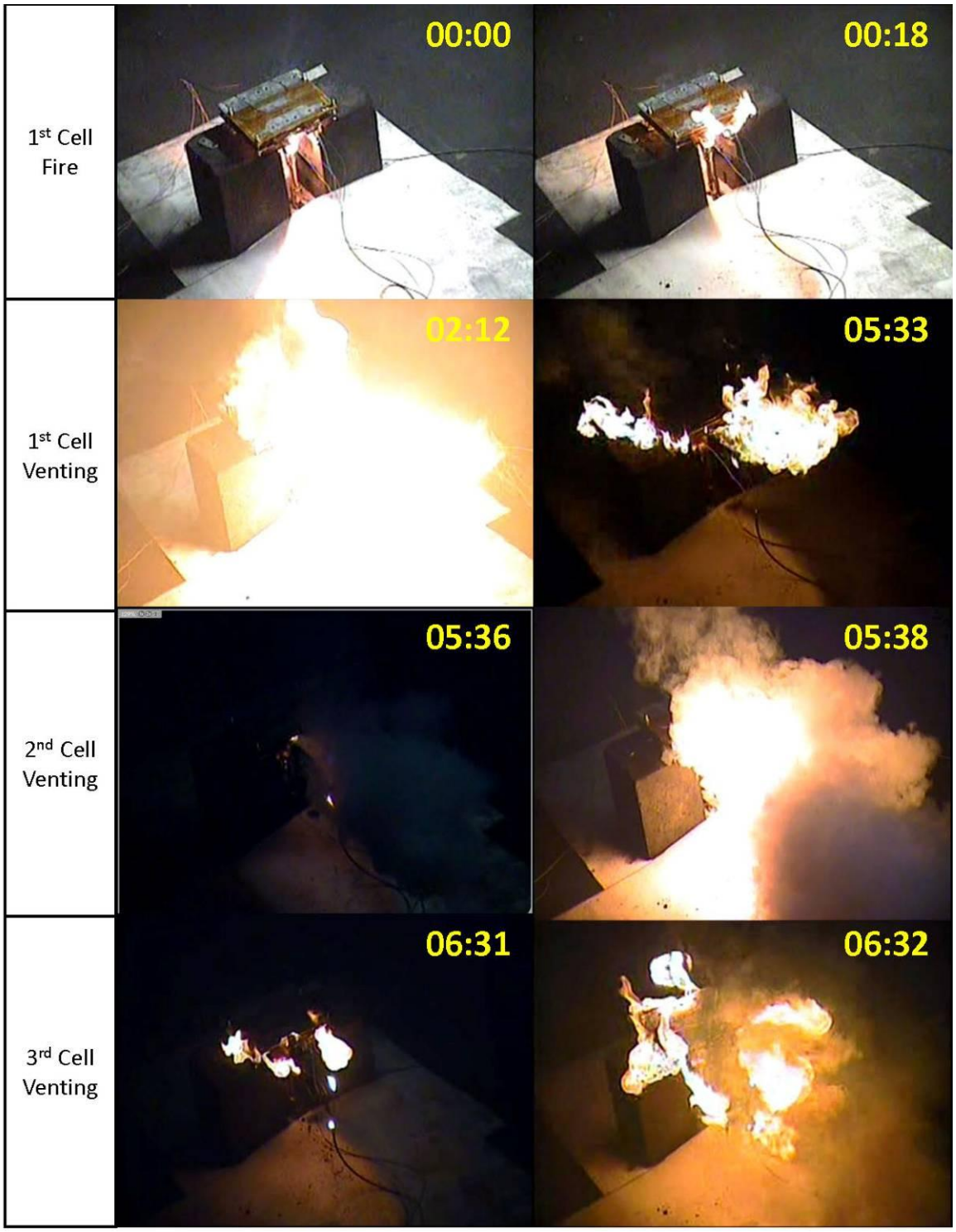

Figure 13: Cell S/Ns O00019, M00043, M00044 Flame Test Video Screen Captures

3 Test 2 & 3- Exposure to Low Thermal Flux (Heat Tape)

3.1 Introduction

The low thermal flux test was performed as a means of providing a slow uniform rise in cell temperature utilizing high temperature heat tape. The tests performed are outlined in Table 2. Three single cell heat tape tests were performed to determine the nano titanate cells' venting temperatures and resulting reactions. The two single cell heat tape test and the three cell test, configured in series, were performed within a pressure vessel, also known as a test bullet, in order to measure both the venting pressure of the cells and to allow for gas samples of the vent gases to be collected. In addition to the venting pressure, Test 7 & 8 were performed to compare the resulting pressures and types of venting gases produced according to their charge capacity (i.e. overcharged and at the low voltage cutoff).

Test	Serial Number	Test Location	Test Description
1	I00014	Performed in test cell	Determine venting temperature
2	O00002	Performed in test cell	Determine venting temperature
3	L00020	Performed in test cell	Determine venting temperature
4	L00003	Performed in pressure bullet	Determine venting pressure & vent gas analysis
5	N00023	Performed in pressure bullet	Determine venting pressure & vent gas analysis
6	N00026 N00017 N00018	Performed in pressure bullet	Determine venting pressure
7	O00016	Performed in pressure bullet	Determine venting pressure & vent gas analysis at low cut off voltage
8	N00004	Performed in pressure bullet	Determine venting pressure & vent gas analysis which occurs during an overcharge (no heat tape)

Table 2: Low Thermal Flux Cell Test Outline

3.2 Test Method

As previously described, the cells for the following test have been compressed between aluminum plates and fully charged prior to testing; however, unlike the test in section 2, the plates were wrapped with high temperature heat tape, an insulating fiberglass matt and then tightly wrapped with fiberglass tape to ensure adequate contact between the heat tape and the aluminum plates, Figure 14. Tests 1-3 of Table 2 were conducted in a test room equipped with audio and video feeds. The cells were configured with four thermocouples (2 per side) which monitored the aluminum plate temperature beneath the heat tape.

Figure 14 Altairnano Li-Ion Nano-Titanate Heat Tape Test Setup (S/N O00002)

Tests 4-8 of Table 2 were conducted in a pressure vessel, termed the pressure bullet, equipped with electrical feedthroughs for wiring (i.e. wires for thermocouples and heat tape) a pressure sensor, and a gas sampling port. The heat tape, fiberglass matt, and fiberglass tape were arranged in the same configuration as in Test 1-3. Figure 15, is an example of the Test Bullet setup.

Figure 15: Altairnano Li-Ion Nano-Titanate Heat Tape Test Setup in the Test Bullet

3.3 Cell Test 1-3: Results and Discussion

A constant current was supplied to the cell's heat tape providing an average temperature rise of ~12°C / min at the surface of the aluminum plates. The key transition points observed during the test video of S/N I00014, and representative of all three tests, are depicted in Figure 16. For reference, time zero represents a baseline showing the cell prior to the application of heat. At time 0:44 (time is formatted as min:ss), the electrolyte was forced out of the cell, in a gaseous phase, and condensing on the thermal matt forming an observable pool. At time 6:08, the cell violently vented electrolyte; however, no flames were observed. The last frame, at time 9:50, shows the resulting burn marks on the thermal matt. It was observed that during each of the three test venting occurred on the electrical tab side of the cells.

During cell heating a sharp drop in each cell's voltage, as can be seen in the plots of battery Temperature vs. Voltage, Figure 17, at which time, the current supplied to the heat tape was removed. The average aluminum compression plate temperature at the point of the voltage drop for all three tests was found to be ~206°C. Table 3 list the individual plate temperatures observed during testing. After the batteries voltage dropped the cell continued to heat until the electrolyte vented. The average maximum temperature of 319°C was observed at the plate surface during the venting process. Figure 18 shows the before and after photographs of cell S/N I00014.

Cell Test	S/N	Average Temperature at Voltage Short (°C)	Maximum Temperature at Voltage Short (°C)	Maximum Temperature (°C)
1	I00014	204.3	216.4	308.4
2	L00020	205.5	222.2	322.3
3	O00002	207.6	252.4	326.9

Table 3: The cell temperatures observed during the low thermal flux (Heat Tape) Test

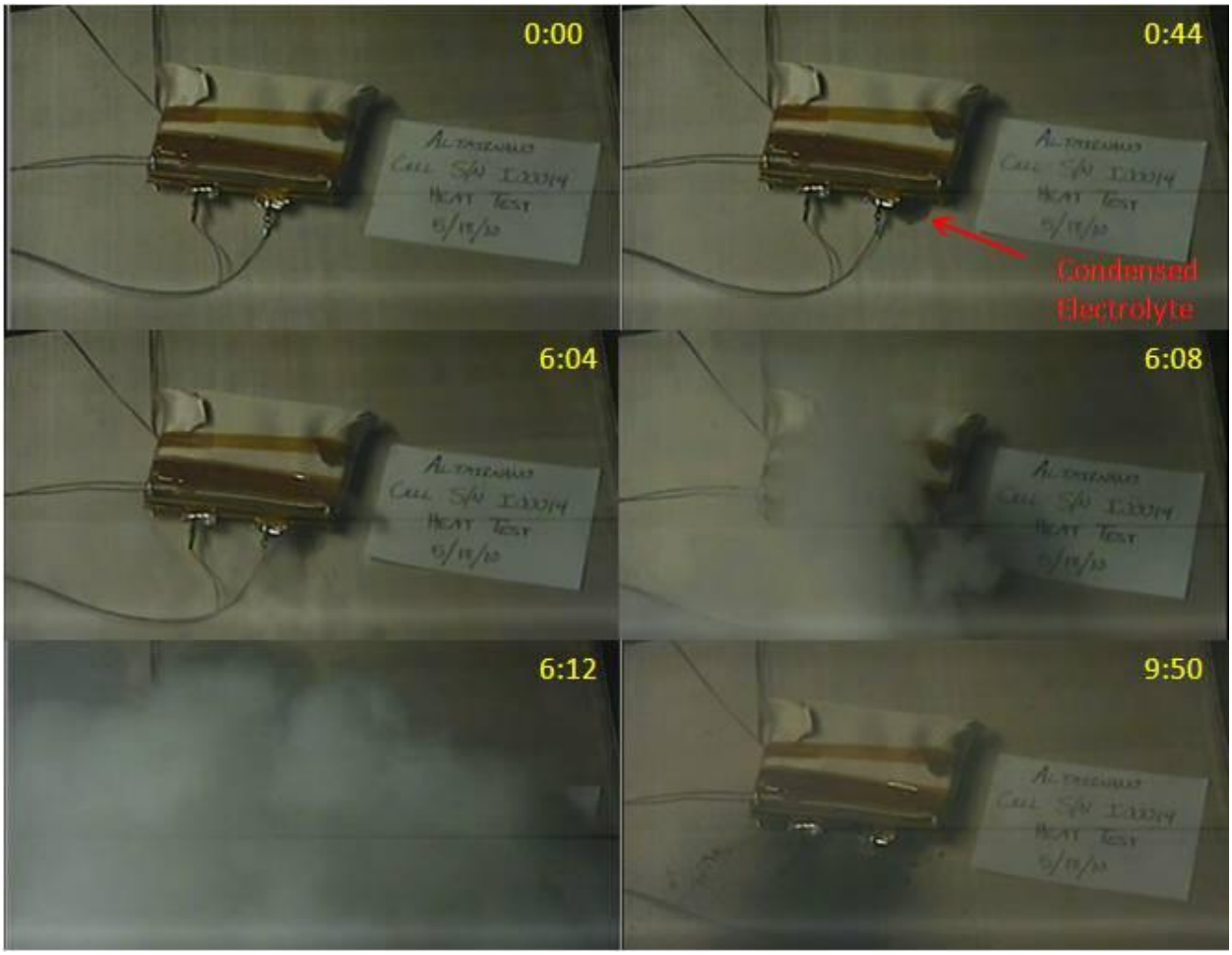

Figure 16: Cell S/N I0004 Heat Tape Video Captures

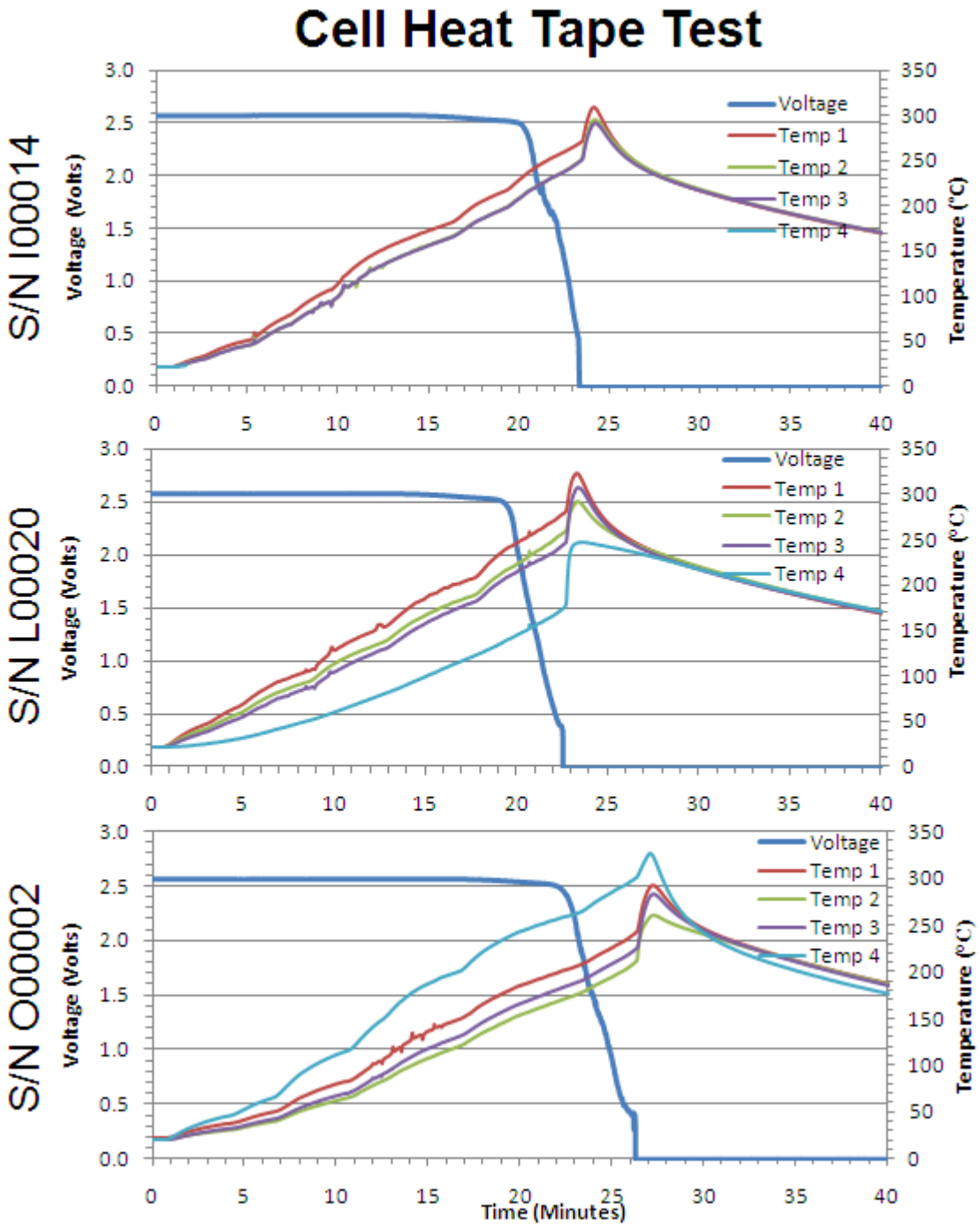

Figure 17: Temperature plots for the low thermal flux (Heat Tape) Test

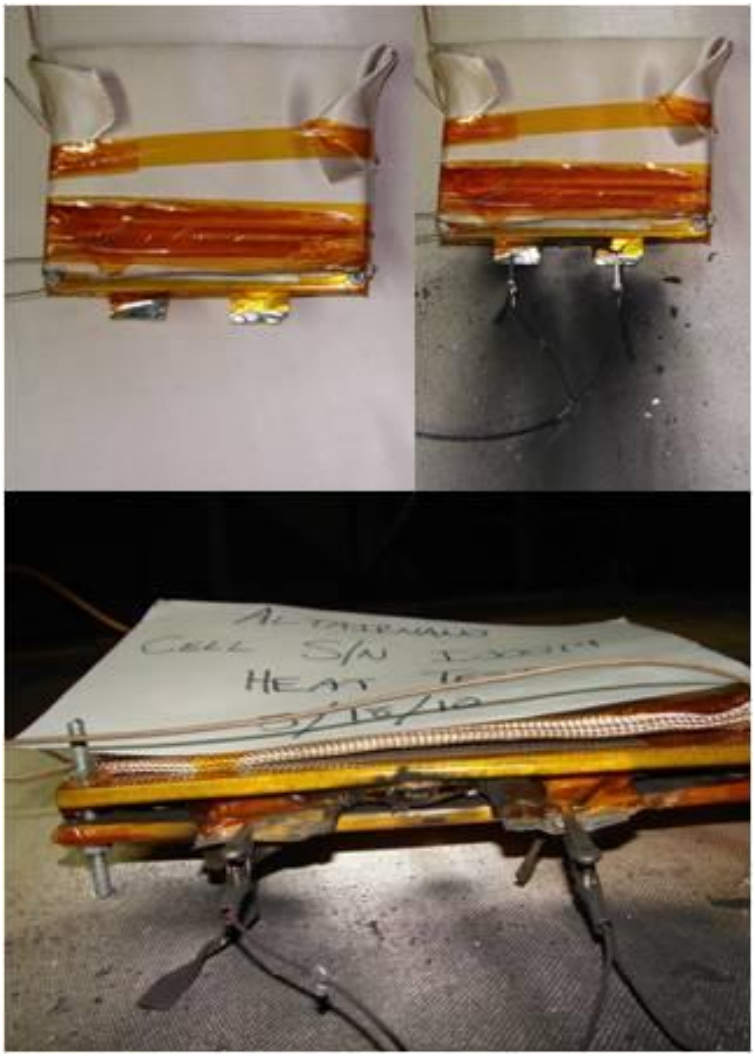

Figure 18: Altairnano Cell S/N I00014 Heat tape test before and after photos

3.4 Cell Test 4-8: Results and Discussion

As with Cell Test 1-3, a constant current was supplied to the cell's heat tape in Cell Tests 4-7, providing an average temperature rise of ~12°C / min at the surface of the aluminum plates. After observing a sharp drop in each cell's voltage, as can be seen in the plots of battery Temperature vs. Voltage, Figure 20 & Figure 21 (pgs 22 & 23) the current supplied to the heat tape was removed. The average battery temperature at the point of the voltage drop for Test 4-6, was found to be 190°C. Table 4 list the individual battery temperatures recorded during testing. After the batteries' voltages dropped, for tests 4-6, the cells quickly heated due to internal processes until the electrolyte vented. The average maximum temperature of 345°C was observed at the plate surface during the venting process. Figure 19 (page 21) shows the before and after photographs of cell S/N L00003.

Cell Test	S/N	Average Temperature at Voltage Drop (°C)	Maximum Pressure (psi)	Maximum Temperature (°C)
4	L00003	191	19.7	270
5	N00023	190	18.2	330
6	N00026 N00017 N00018	217 238 281	31.5	390
7	O00016	189	11.3	435
8	N00004	NA	2.5	82

Table 4: The cell temperatures observed during the low thermal flux (Heat Tape) Test

To gain insight into the impact of a cell's state of charge on the venting reaction and vent gas byproducts, the cells in Cell Test 7 & 8 (S/N O00016 & N00004) were tested at the recommended low cut off voltage and at an overcharged voltage, respectively, as opposed to a nominal charge capacity. The cell voltage recommendations, as found on the product specification sheet, and the cell's charge configuration prior to testing can be found in Table 5.

Cell Test 7 (S/N O00016) was heated via heat tape under the same configuration as cell test 1-6, and resulted in a maximum vent pressure of 11.3 psi. This is nearly half the maximum venting pressure observed during Cell Test 4 & 5. The lower pressure is likely due to the fact that Cell 7 had less stored energy and therefore less energy that could be converted to heat during the venting/shorting event.

Cell Test 7 Testing Configuration (SN O00016)	
Voltage Upon Receipt	1.92 V
Capacity Discharged	6.21 Amp hr
Initial Testing Voltage	1.87 V
Temperature at Vent	183 ℃
Recommended Cut Off Voltage (From Spec)	
Range -40 to +30	1.5 V
Range +30 to +55	2.0 V

Table 5: Cell Test 7 setup configuration and test data

As is typical for Li-ion batteries, charging them past there recommended capacity can have serious repercussions such as unexpected and violent cell/module venting events. To simulate this scenario Cell Test 8 was not heated with heat tape, such as Cell test 1-7, but instead overcharged within the test bullet. The batteries initial voltage, final voltage, and total charge past the minimum voltage can be found in Table 6. Plots of the batteries' voltage, charging current, temperature, and pressure can be found as Figure 22.

S/N	Voltage upon Receipt	Added Energy	Cell Voltage	Temp at vent
N00004	2.03 V	85 Watt hr 1037 Watt hr	4.74 V 1.51 V	50.72 ℃

Table 6: Cell Test 8 (Overcharge Test) Test Data

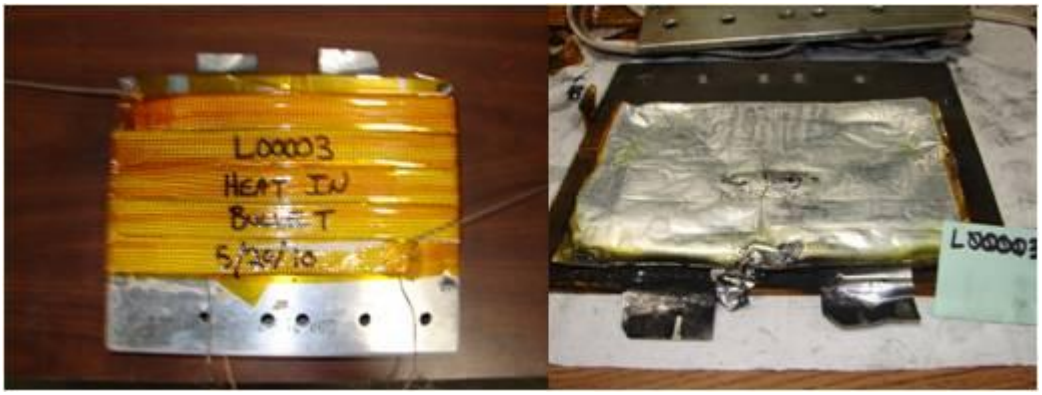

Figure 19: Heat Tape Test (Pressure Bullet) Before and After Photos

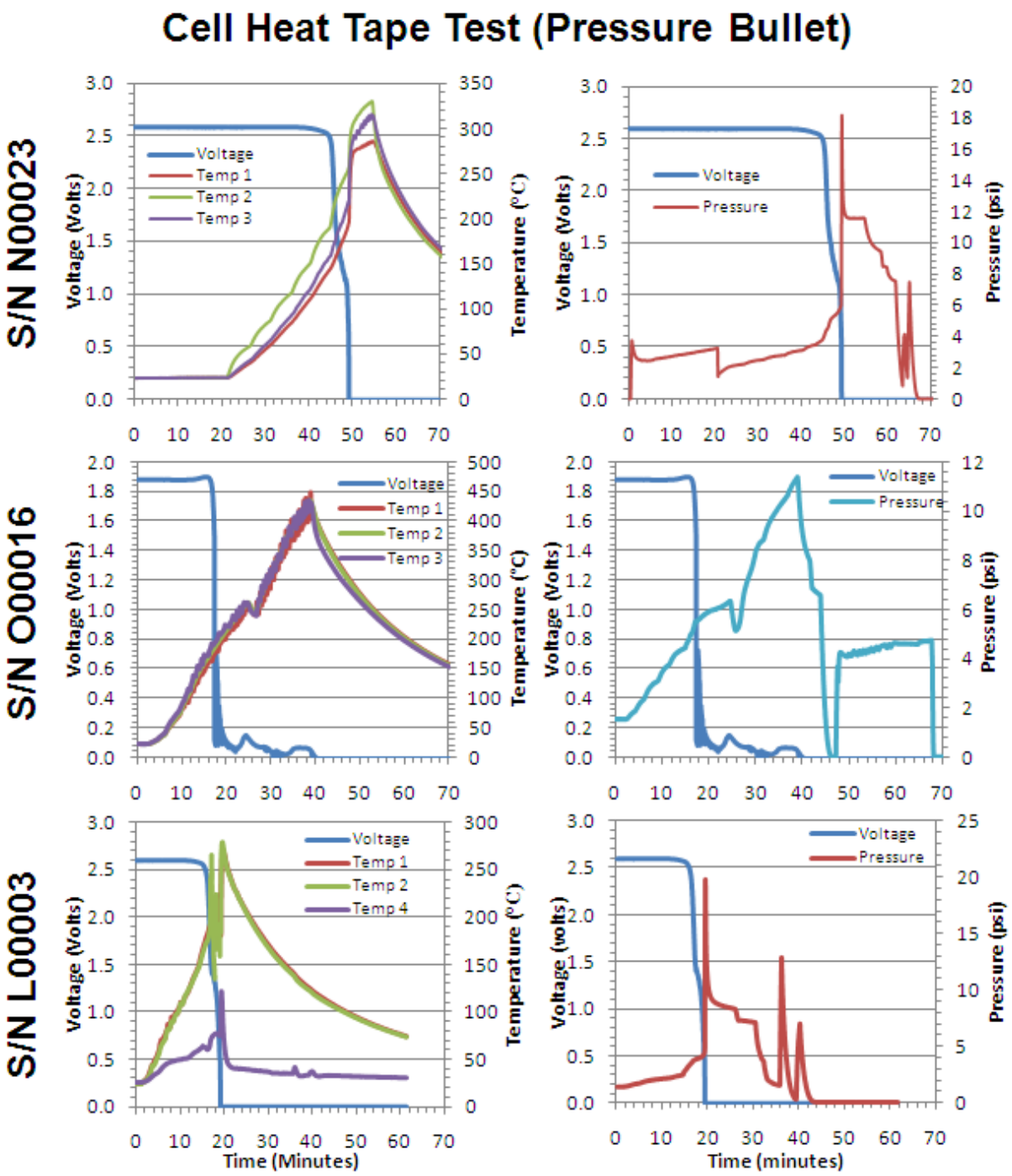

Figure 20: Low Thermal Flux Test Plots - Single Cell in Test Bullet

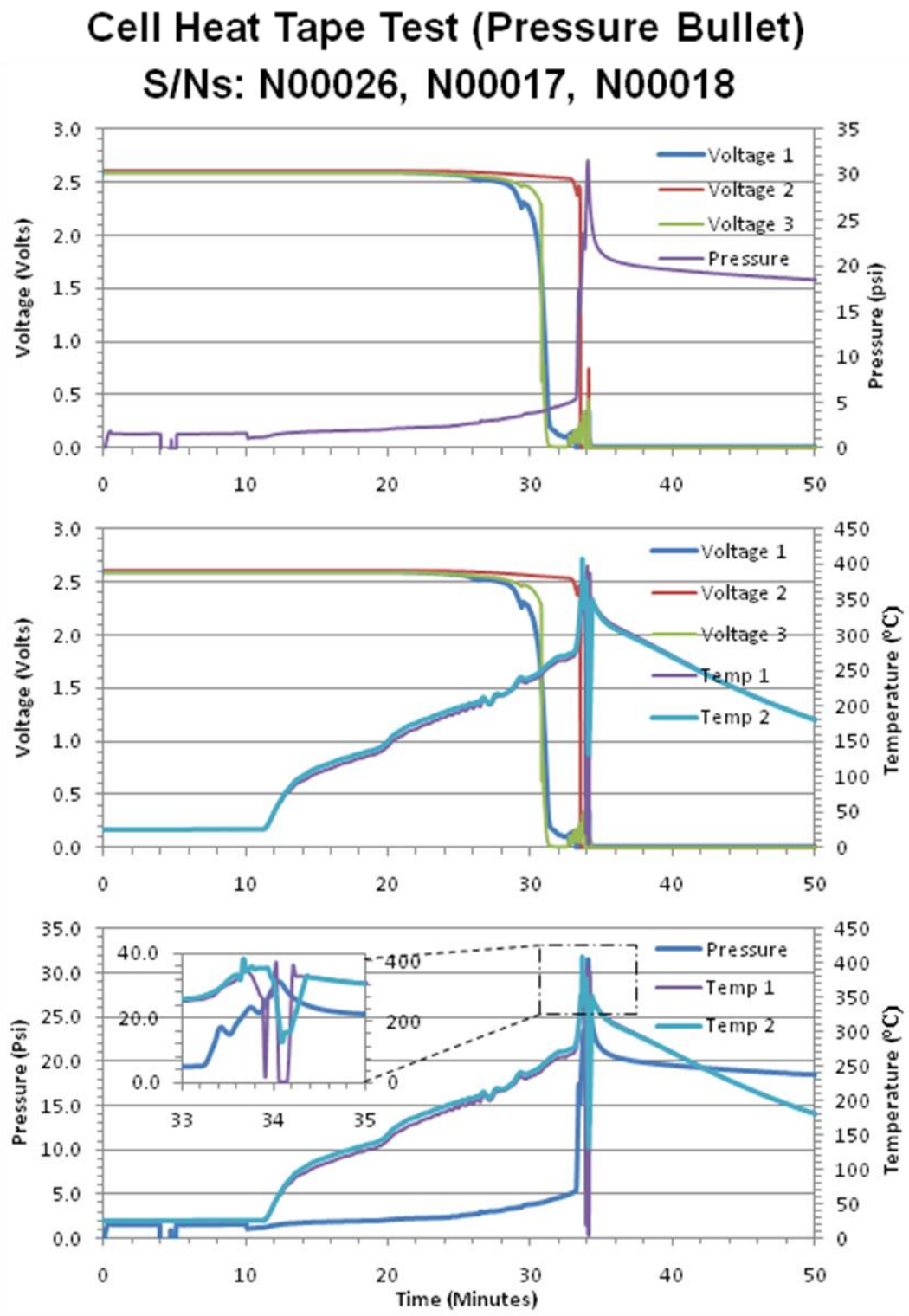

Figure 21: Low Thermal Flux Test Plots - Three Cells in Test Bullet

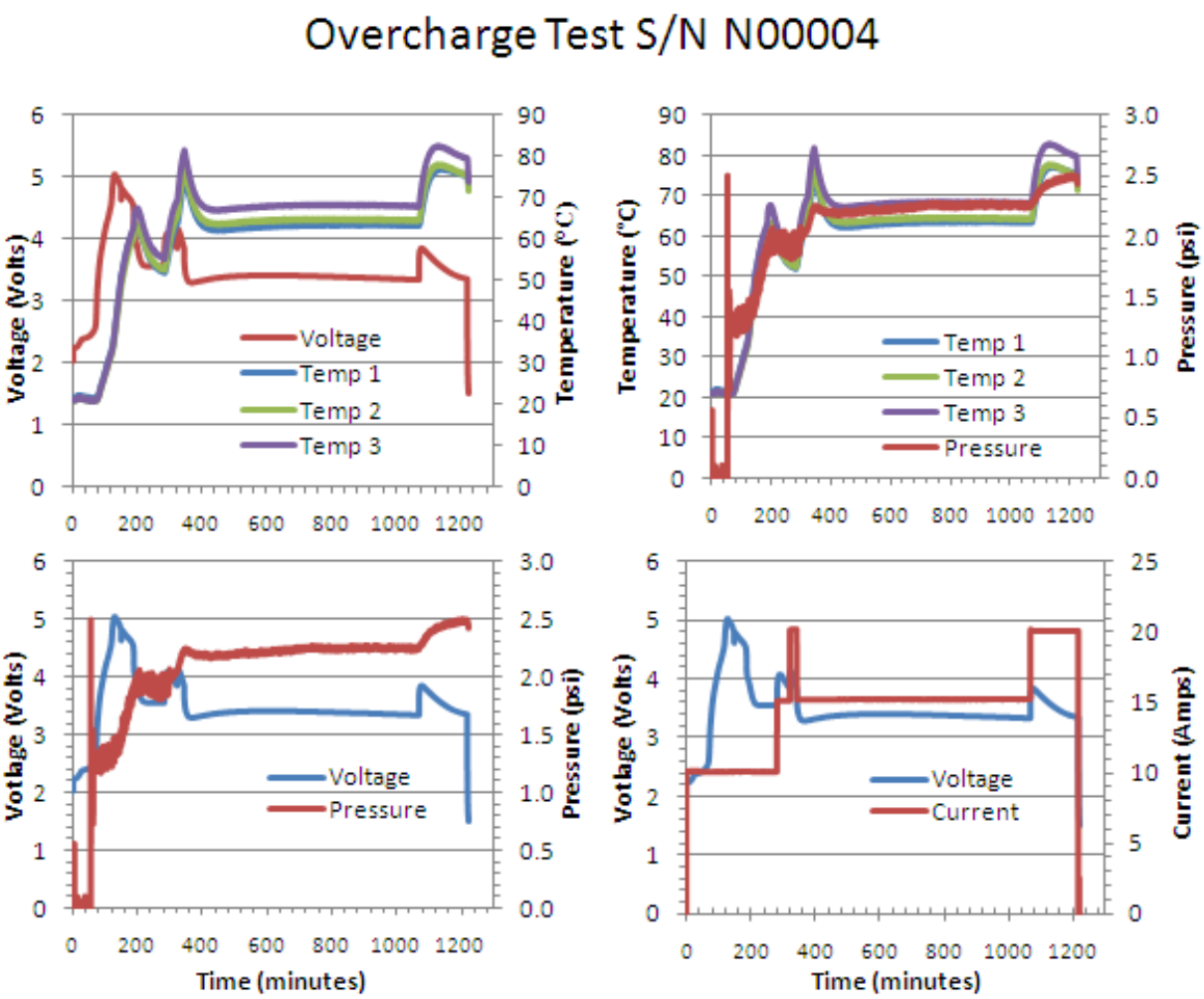

Figure 22: Overcharge Test Plots - Single Cell in Test Bullet

4 Test 2 & 3 Cont'd - Vent Gas Analysis

4.1 Gas Sample Collection Method

During Cell Test 4-8 (Section 3, Test 2) gas samples were collected utilizing 3L Tedlar gas sampling bags and a sampling port equipped on the pressure vessel. To prevent the loss of gaseous compounds of interest, either due to side reactions within the vessel or due to gas condensation, gas samples were immediately taken following a venting occurrence. The Tedlar bag was connected to the test bullet and filled with the venting byproducts ensuring that the gas valve on the bag was properly used thus preventing the loss of gas samples and/or contamination by atmospheric gases.

Each gas sample bag was injected with 10.0 mL of gaseous 99% N_2O at atmospheric temperature and pressure. The 99% N_2O was required to calibrate the response of a Gas Chromatogram Mass Spectrometer (GC/MS). Using a gas syringe, 0.5 cc gas samples were removed from the bags and injected into the GC/MS. The resulting peak areas were compared with the calibration injections to yield estimates of the bag volume[*]. These volumes range from 2.25 to 3.8 liters, they are listed in Table 7.

4.2 Vent Gas Analysis: Quantification of Hydrofluoric Acid

After gas sampling for GC/TCD runs, each bag was injected with 25.0 mL of 15% KOH. The KOH solution acts as the 'absorbent' for the HF, very efficiently converting the HF into dissolved KF. The extraction was conducted for about 3 days.

A fluoride ion-selective electrode was utilized to analyze 4.0 mL samples of the KOH extracts after neutralization with 35% HNO_3 and dilution with a 15% ammonium acetate buffer to 50 mL. The electrode calibration was checked with a range of standard solutions to give a Nernst-type calibration equation:

$$\text{Voltage} = [-58.2 \times \log(\text{concentration}) - 366.3]\ \text{mV}$$

which is used to compute the HF concentrations from measured voltages. The slope of (-58.2 mV/decade) is well within the 'normal' range.

The measured KF levels for the test samples, along with computed HF concentrations in the gas sample are given in Table 7.

[*] In the following computations it is assumed that the internal pressures of the gas sample bags are at standard atmospheric pressure.

Test Sample	Sample mV	Volume of Gas sample (L)	[F^-] in KOH extract (ppm)	Grams of HF (total) in sample*	Partial volume of HF** in gas sample (L)	[HF] in gas sample (ppm) (v/v)
L0003	-448.7	2.25	26.050	2.14E-03	0.00262	1160
N00004	-358.4	2.42	0.732	6.02E-05	7.35E-05	30.4
000016	-419.3	3.80	8.141	6.69E-04	0.000818	215
N00023	-451.5	3.30	29.102	2.39E-03	0.00293	975
blank	-314.0	[nom. 3 L]	[0.126]	[1.04E-05]	[1.27E-05]	[3.8]

*this computation allows for: 1) a sampling fraction of (4cc / 25cc), and 2) a dilution factor of (50cc/4cc) used in the fluoride analysis, giving a net analysis scaling factor of (78.125 x).
**this was computed assuming the gas samples were collected at standard temperature and pressure.

Table 7: Vent Gas (Hydrofluoric Acid) Analysis Data

The bottom row of the table, the solution 'blank' for the fluoride electrode measurement, establishes the practical detection limit of the method and was found to be ~4 ppm HF for these types of gas samples.

The difference between measured HF levels for the test samples L0003 and 00023 is 18%: reportedly these were duplicated tests, but this difference is not large considering the nature of the testing and analysis.

The other thing to note is the high level of HF in these two tests, amounting to 0.1 % or more, in gas-volume terms. This is a relatively high level for a toxic gas such as HF. Also, note that all tests gave some level of detectable HF in excess of the estimated detection limit of about 4 ppm.

Finally, it is noted that colors developed for all the KOH solution extracts, except for the N00004 test. The colors were yellowish brown, being quite intense for test 000016, with lighter colors of similar intensities for N00023 and L00003, Figure 23. Interestingly, the latter two produced the very high HF levels, while the level for O00016 was substantial but lower than these two. It should not be assumed that the colors being extracted by the KOH are necessarily due to reaction with the KOH: it could be that these unknown colored substances, originating in the gas samples, simply are soluble in the aqueous KOH, and may be soluble in water, as well.

Figure 23: Cell Vent Test - Hydrofluoric Acid Vent Gas Samples

4.3 Vent Gas Analysis: Qualitative Volatile Organics

The following gas characterization was performed using 1 cc of gas introduced into a specialized GC/MS. These data are semi-quantitative and the reported percentage is a percent of the total ion chromatogram (TIC).

Battery SN O00016

- 1-Propene, thaol,1,1-dimethoxy ethane, 1,3,5Trifluorobenzene, Benzene, Styrene, Carbonic acid ethyl methyl ester (39.4 % of TIC), 1,4 Dioxane, Toluene, 2,4-Dimethyl-1-heptene , 1-methyl-2pentyl Cyclopropane.

Battery SN L00003

- 1- Propene, Ethyl Cyclopropane, 1- Hexene, 1,2,3,-Trifluorobenzene, Benzene, Isopropylcyclobutane, Heptane, Carbonic acid ethyl methyl ester (48.92 % of TIC), Toluene, 1-Octene, Carbonic acid diethyl ester (3.33 % of TIC), 1-Nonene, Nonane, 1-Decene.

Battery SN N0004

- Fluoro Ethane, Butane, Acetic acid methyl ester, Ethyl Acetate, Carbonic acid dimethyl ester (12 % of TIC), carbonic acid ethyl methyl ester (56.7 % of TIC), Carbonic acid diethyl ester (17.8 % of TIC).

Battery SN N00023

- 1-Propene, Methoxy Ethane, Ethyl Cyclopropane, 1-Hexene, 1,2,4 Trifluorobenzene, Benzene, 4-methyl Cyclopentene, 1-Heptene, Heptane,

Carbonic acid ethyl methyl ester (49.6 % of TIC), Toluene, 1-Octene, Octane, 1-Nonene, Nonane, 1-Decene

4.4 Vent Gas Analysis: Low Molecular Weight Vent Gases

Utilizing a Perkin-Elmer Autosystem XL GC and a Perkin-Elmer GC with a TurboMass Mass Spectrometer, vent gas samples were quantitatively analyzed for 11 possible compounds, nine of which were identified, Table 8. Two unknown compounds (peaks) with retention times of 8.57 min and 9.94 min were noted on the Chromatograms. The GC/MS library (NIST) attempted to identify the compounds as carbonic dihydrazide and fluoro-ethane, respectively. The compounds were present in trace amounts well below 0.5%.

Low Molecular Weight Vent Gas Concentration (Volume %)								
S/N	Methane (CH_4)	Carbon Dioxide (CO_2)	Hydrogen (H_2)	Oxygen (O_2)	Ethene (C_2H_4)	Ethane (C_2H_6)	Propene (C_3H_6)	Propane (C_3H_8)
N00004	0.78	2.81	0.85	0.21	0.05	0.49	BDL	0.01
L00003	0.37	11.70	5.96	0.56	0.69	0.04	0.08	0.03
O00023	0.62	12.18	6.02	0.78	0.80	0.05	0.06	0.02
000016	0.56	9.44	0.53	0.27	4.67	0.05	0.05	BDL
Notes: Measurements below sensitivity levels of the instruments are listed as Below Detectable Limits (BDL).								

Table 8: Vent Gas (Low Molecular Weight Gases) Analysis Data

5 Test 4 – Electrolyte Flash Point Test

Altairnano requested NSWC Crane perform both open and closed cup flash point testing on ethyl methyl carbonated electrolyte used within their Altairnano Mark I modules/cells). Table 9 lists the properties from the Novolyte Technologies Data Sheet. The testing methods used were in accordance with ASTM D92 and D93. Standard reference material was obtained from Koehler Instruments for both open and closed cup testing. The instrument was first verified with the standard reference material utilizing the recommended heating rates of ASTM D92 and D93. Table 10 summarizes the results of both tests.

Novolyte Technologies Electrolyte Safety Data Information		
Commercial Product Name	SSDE-AN-42	
General Flashpoint (estimated)	24°C	
Hazardous Components	CAS No.	Concentration
Ethyl methyl Carbonate	623-53-0	< 60%
Alkyl Carbonate	-	< 30%
Lithium Hexafluorophosphate	21324-40-3	< 16%

Table 9: Electrolyte Specifications Data

Observed Flash Point		
Test Type / Run	Open Cup	Closed Cup
Run #1	36.4°C	32.5°C
Run #2	36.3°C	30.2°C

Table 10: Electrolyte Flash Point Data

6 Test 5 - High Temperature Module Test (Fuel Fire)

6.1 Introduction

On July 22nd 2010, two Altairnano Li-ion nano-titanate modules were subjected to ~20 minutes of direct high temperature flames generated by 200 gallons of burning kerosene at the Ordnance Test Area (OTA) at NSWC Crane to determine the batteries reactions in a worst case scenario fire event. The Mark 1 modules safely burned with the speed of the combustion process such that gases were not liberated rapidly enough to cause an explosion. Additionally, external thermocouples support the latter statement with neither a supersonic nor subsonic shock wave being recorded. All cells appeared to vent and each cell had a voltage of 0V at the conclusion of testing.

6.2 Test Method

Prior to testing, two Altairnano modules were fully charged using the following procedure: The modules (S/N 095-08259002 & S/N 065-08260003) were charged at a current rate of 300 amps, removing the charging current when any of the cell voltages reached 2.8 volts. After removing the charging current the voltage was allowed time to stabilize and charging continued at a lower current rate of 100 amps until any of the cell voltages, again, read 2.8 volts. The batteries were equipped with multiple thermocouples, some of which were potted internal to the battery at the point of manufacturing and others added to their outside casings. All exposed wires were wrapped in fiberglass matting and fiberglass tape in order to help prevent the loss of connection due to the wires melting,

Figure 24 (left image).

The fuel fire consisted of an ~10 foot diameter steel ring welded to a bottom steel plate and capable of holding a liquid,

Figure 24 (right image). The fuel fire ring was filled with ~ 8 inches of water, which provided a flat surface for the fuel, and 200 gallons of kerosene. In the center of the fuel pit was a large steel stand, where the batteries were placed for testing, with gratings beneath it to allow for adequate flame/heat transfer to the batteries.

Testing was conducted at the outdoor Ordnance Test Area (OTA) at NSWC Crane. All personnel were removed from the testing location and allowed to view the test from a protective shelters equipped with 3 different video feeds. The test area was equipped with multiple shockwave sensors spread radially from the center of the fuel fire pit.

Figure 24: Fuel Fire Test Setup Photos

6.3 Results and Discussion

The fuel fire test demonstrated the effects of subjecting the battery modules to high temperatures created by burning kerosene fuel. Compared to typical Li-Ion batteries, the Altairnano nano-titante modules degraded in a safer manner with the no observable explosions or rapid decimation. Additionally, testing revealed no detectable shock waves. As calculated from the external thermocouple data, Figure 25, the average and maximum temperatures subjected to the batteries was 1620°F and 2700°F, respectively.

Despite being wrapped in high temperature fiberglass insulating material the internal thermocouple and voltage monitoring wires were destroyed during the first few minutes following ignition of the fuel fire. A review of the test video revealed that the modules started to vent, evident by the sound of escaping gaseous electrolyte, after exposure to ~5 minutes of heat.

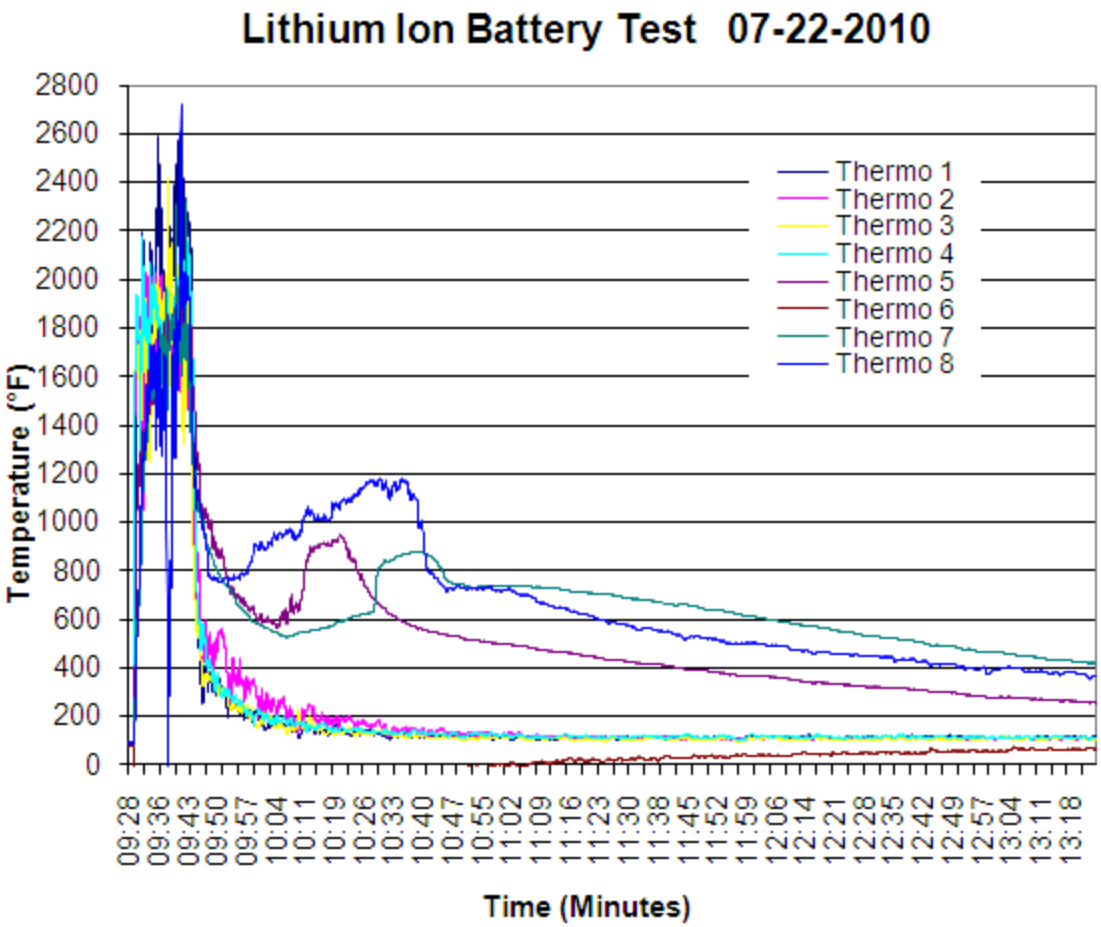

Figure 25: Mark I Module Fuel Fire Test – External Thermocouple Plots

Figure 26: Mark I Module Fuel Fire Test- Mark I Modules after Testing

7 Test 6 - High Temperature Module Test (Heat Tape)

7.1 Introduction

The low thermal flux module test was performed to observe the effects on a battery when subjected to a slow uniform rise in module temperature utilizing high temperature heat tape. A single Mark I module was tested to determine the venting temperature as well as the heat flux throughout the module. It was observed that even though the heat tape's current was removed after the first venting event, the module's core temperature steadily increased causing additional cells to vent.

7.2 Test Method

As previously described, the module for the following test was fully charged prior to testing. After the module was charged and allowed time to cool to room temperature, it was wrapped with high temperature heat tape, an insulating fiberglass matt, and then tightly wrapped with fiberglass. This process to ensured adequate contact between the heat tape and the module, Figure 27.

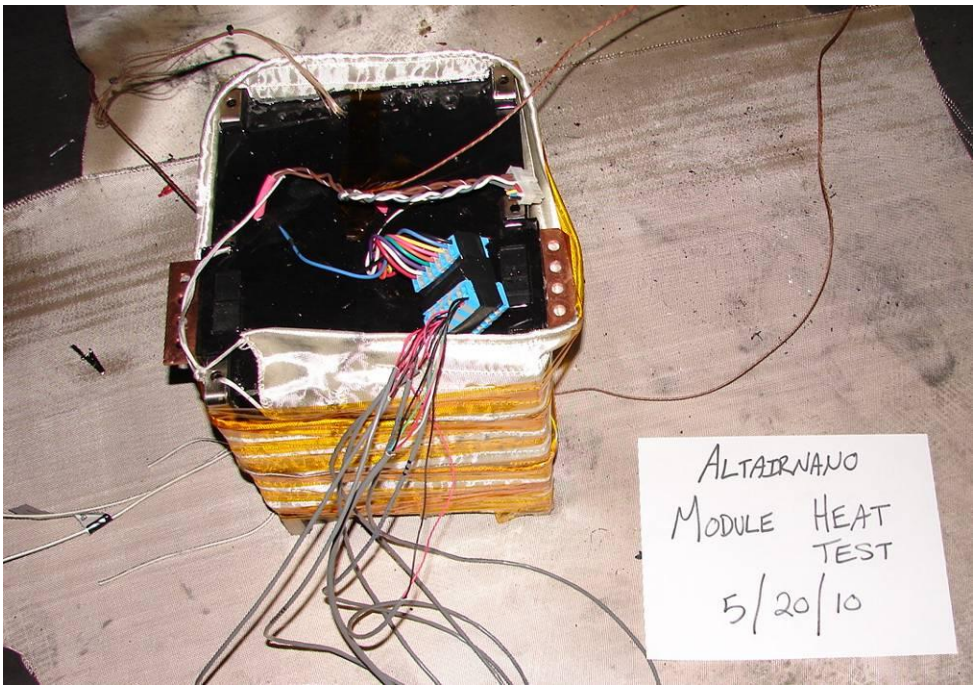

Figure 27: Mark I Module Heat Tape Test Setup

The battery was setup within a test cell equipped with a scrubber system and audio/video feeds. Twelve internal and four external thermocouples were connected to the data acquisition system and the battery. Table 11 describes the external thermocouple layout.

Thermocouple Connection Description	
Thermocouple	Position/Connection
External	
1	Side of Module
2	Top of Module
3	Top of Module
4	Bottom of Module

Table 11: Module Heat Tape Test -Thermocouple Placement

7.3 Results and Discussion

As seen in top two plots of Figure 28, each drop in cell voltage correlates with a sharp rise in thermocouple temperature. The lower figure shows the external thermocouple temperature which correlates with the first venting event. After the initial rise in thermocouple temperature the thermocouples behaved erratically and the data was filtered thereby removing the spikes in temperature that were likely due to the thermocouples being shorted out by condensing electrolyte.

The current to the high temperature heat tape was turned off at the start of the first venting event. Thereafter, the heat propagated inwards causing a chain reaction whereby each adjacent cell vented, transferred heat to the next adjacent cell, and so forth until all cells had vented. Due to the lose in the video feed, caused by dense smoke created by the first venting event, and due to the erratic behavior of the external thermocouples, it has been undetermined if the module caught fire.

A visual investigation after testing, Figure 29, showed that the epoxy had reached a critical temperatures and became unstable losing its rigid form (lower right image). Additionally, a large amount of a viscous liquid, possibly being a decomposition byproduct of the modules epoxy, pooled around the bottom of the module.

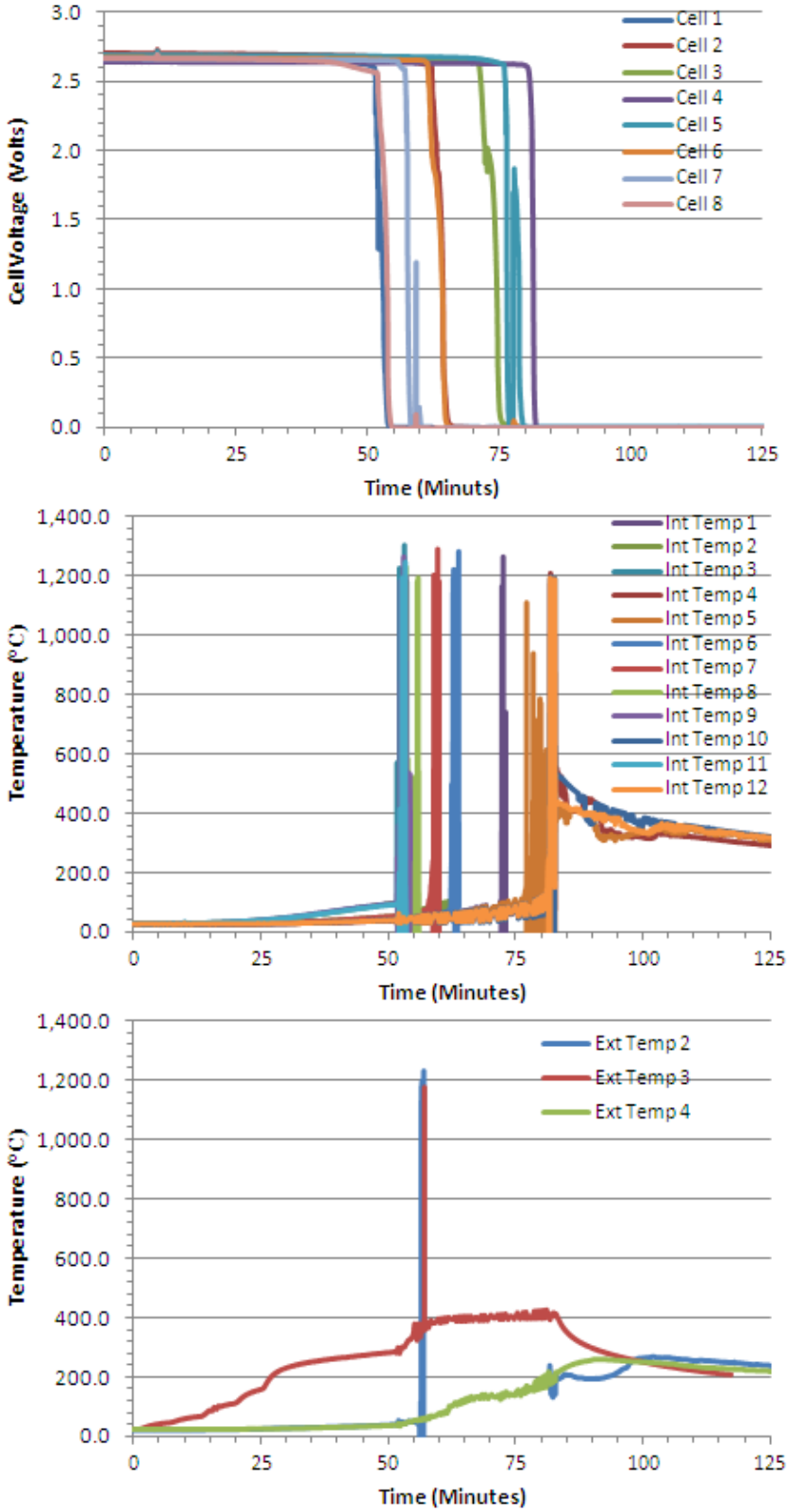

Figure 28: Mark I Module Heat Tape Test - Data Plots

Figure 29: Mark I Module Heat Tape Test - Module after Testing

8 Test 7 - Fire Suppression Testing

8.1 Introduction

The objective of the following three tests was to determine the effectiveness in extinguishing a simulated module battery. The tests performed are as follows: 1) water dispersed from an overhead sprinkler system, 2) carbon Dioxide (CO_2) dispersed from two 10 lb fire extinguishers, 3) FM200, a gaseous Halon replacement, dispersed from a single nozzle within the room.

8.2 General Test Setup

The battery modules were fully charged prior to testing as previously described. Data acquisition included 12+ thermocouples (both internal and external to the module), 8 cell voltage lines, and both a video and sound feed within the test chamber. The internal thermocouples were installed during battery manufacturing and their method of installation is described in Figure 30. Their placement and quantity varied per module serial number. A detailed schematic outlining the thermocouple locations within the modules can be found in Appendix C: Mark I Module Internal Thermocouple Schematic.

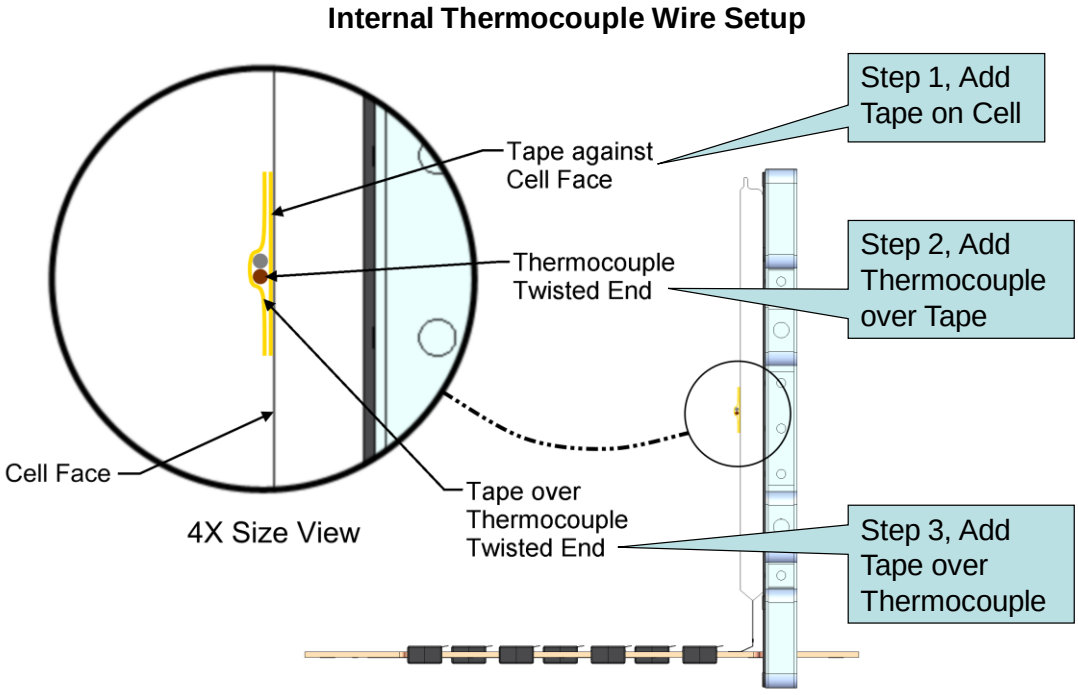

Figure 30: Mark I Module Internal Thermocouple Installation

The battery modules were placed onto a steel grate 6" above a 25" diameter fire pit. Approximately 2 gallons of methanol, a 1:1 mixture of methanol:water, was poured into the fire pit and ignited remotely moments prior to testing. The quantity of fuel used during testing was such that it provided an ~45 minute burn time.

8.3 CO2 Fire Suppression Test

8.3.1 Test Setup

The extinguishing nozzles from two 10 lb Carbon Dioxide (CO_2) fire extinguishers were centered upon the Mark I Battery module (S/N 065-08261005) atop the fuel fire ring at a 75° angle from one another. The nozzles were radially located at the manufacturer's recommended distance of 6ft. The test setup included remote activation of the fire extinguishers from outside the test chamber. Images of the test setup including both extinguishing nozzles (top left and lower left images) and the battery module atop the fuel pit (top right and lower right images) can be found as Figure 31.

Figure 31: Mark I Module-Carbon Dioxide Extinguishing Test Setup

8.3.2 Results and Discussion

The CO_2 Extinguishing Test, conducted on Tuesday October 19th 2010, demonstrated the effectiveness of gaseous carbon dioxide dispersed from common hand held extinguishers in extinguishing a battery module fire. After subjecting the module to a methanol fire, with a 25 minute expected burn time, the visibility in the test cell reached a critical level due to smoke and the extinguishers were remotely triggered. Test Cell visibility was a necessary parameter in allowing a visual determination of the extinguishers effectiveness. Moments after triggering the extinguishers the fuel fire and some secondary fires on the module, likely to be burning epoxy and/or electrolyte, were quickly extinguished with no observable reignitions. External thermocouples supported these observations. Screenshots from the video of the CO2 test outlining key transitions during the test can be found as Figure 32.

Figure 32: Mark I Module- Carbon Dioxide Extinguishing Video Screenshots

After extinguishing the fire, heat within the battery continued to rise and propagate eventually causing Cells 1 & 8 to vent. This was confirmed in plots of the cell voltage and thermocouples, Figure 33. The plots indicate that after cells 1 and 8 vented their internal temperatures momentarily reached ~1250°C. The heat generated from the venting process slowly transferred into adjacent cells thus causing them to vent. This self-sustaining process of heat generation and thermal propagation continued until all cells vented (~70 minutes after the first venting event). Additionally, the pack voltage was observed to drop coinciding with drops in cell voltages and spikes in thermocouple temperatures. Due to the methanol fire, high temperature vent gases, and condensing electrolyte some thermocouples showed intermittent noise and/or loss of signal during testing.

After testing, a visual inspection of the battery revealed locations on the top of the module where epoxy had melted/burnt away revealing the cells beneath it, Figure 34 . The high temperatures, flames, and pressures generated during a cell venting are likely the cause for the observed holes.

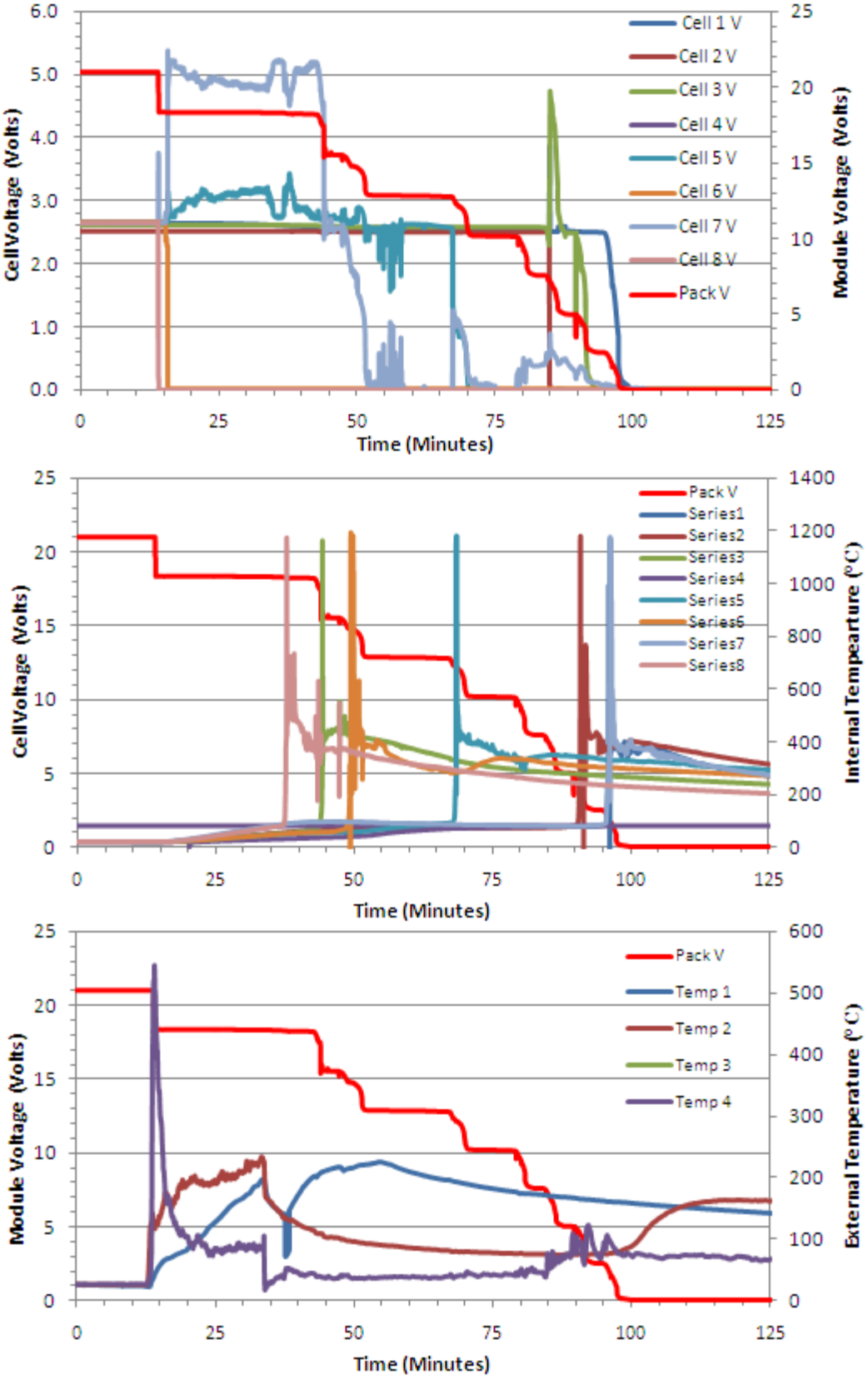

Figure 33: Mark I Module Carbon Dioxide Extinguishing Test Plots

Figure 34: Mark I Module Carbon Dioxide Extinguishing After Test Pictures

8.4 Water Suppression Test

8.4.1 Test Setup

Two sprinklers were located 5 ft above a Mark I Battery module (S/N 065-08273001 88TC), 6 ft from one another, and off centered 3 ft from the battery module atop the fuel fire ring, Figure 35. Two standard response Pendent Sprinklers with the glass bulbs and spring sealing assemblies removed were used with the nominal building water pressure of 60 psi. Additionally, the test setup included remote activation of both the ignition of the methanol fire and the activation of the sprinkler system from outside the test chamber. Images of the test setup including the sprinkler nozzles and the battery module atop the fuel pit can be found as Figure 35.

Figure 35: Mark I Module- Water Extinguishing Test Setup

8.4.2 Results and Discussion

The Water Extinguishing Test, conducted on Thursday October 21st 2010, demonstrated the effectiveness of water administered from two sprinklers in extinguishing a battery module fire. After subjecting the module to 20 minutes of heat from the methanol fire the battery violently vented. Moments after observing the venting event the water sprinklers were triggered with little to no effect upon the fire. While the sprinklers were activated additional cells vented with observable flames propagating from the battery. After running the sprinkler for 3-5 minutes subsequent ignition of venting process were not observed as supported by external thermocouples data. Screenshots from the video of the CO2 test outlining key transitions during the test can be found as Figure 36.

Figure 36: Mark I Module- Water Suppression Test Screen Shots

Due to contamination of the camera lens, from prior testing, the initial screenshot at time 00:00 Figure 36, shows an initial haze which should not be confused as combustion byproducts. As the test continued, visibility quickly diminished until, as shown in screenshot 23:10, a complete loss in visibility was observed. A review of the test video revealed flames originating near the positive terminal, indicated in screenshot 20:21, and is indicative of venting electrolyte. Although this appears to be the origin of the module first catching fire, the first violent venting process at times 20:23-20:26 appeared to be from the top of the battery near the negative terminal.

A graph of Module Voltage and External Thermocouple Temperature Vs. Time, Figure 37 (bottom graph), support the conclusions that after sprinkler activation (at ~20 minutes on the graphs) the water sprinklers required ~3-5 minutes to extinguish the fire at which point no reignitions were observed regardless of other cell venting events. The total time from the first vent until the last cell venting was found to be ~35 minutes as can be deduced from all three graphs. Additionally, as noted previously, the drops in cell voltages (top graph) correlate with the internal thermocouple temperature spikes (middle graph). As reported for the CO2 extinguishing test, the first cell(s) to vent were those that parallel and closest to the sides of the module (Cells 1 & 8). These cells vented within seconds of one another indicating that the module's casing was uniformly heated. Cells continued to vent in order of their location, outside to inside, as heat continued to propagate internally.

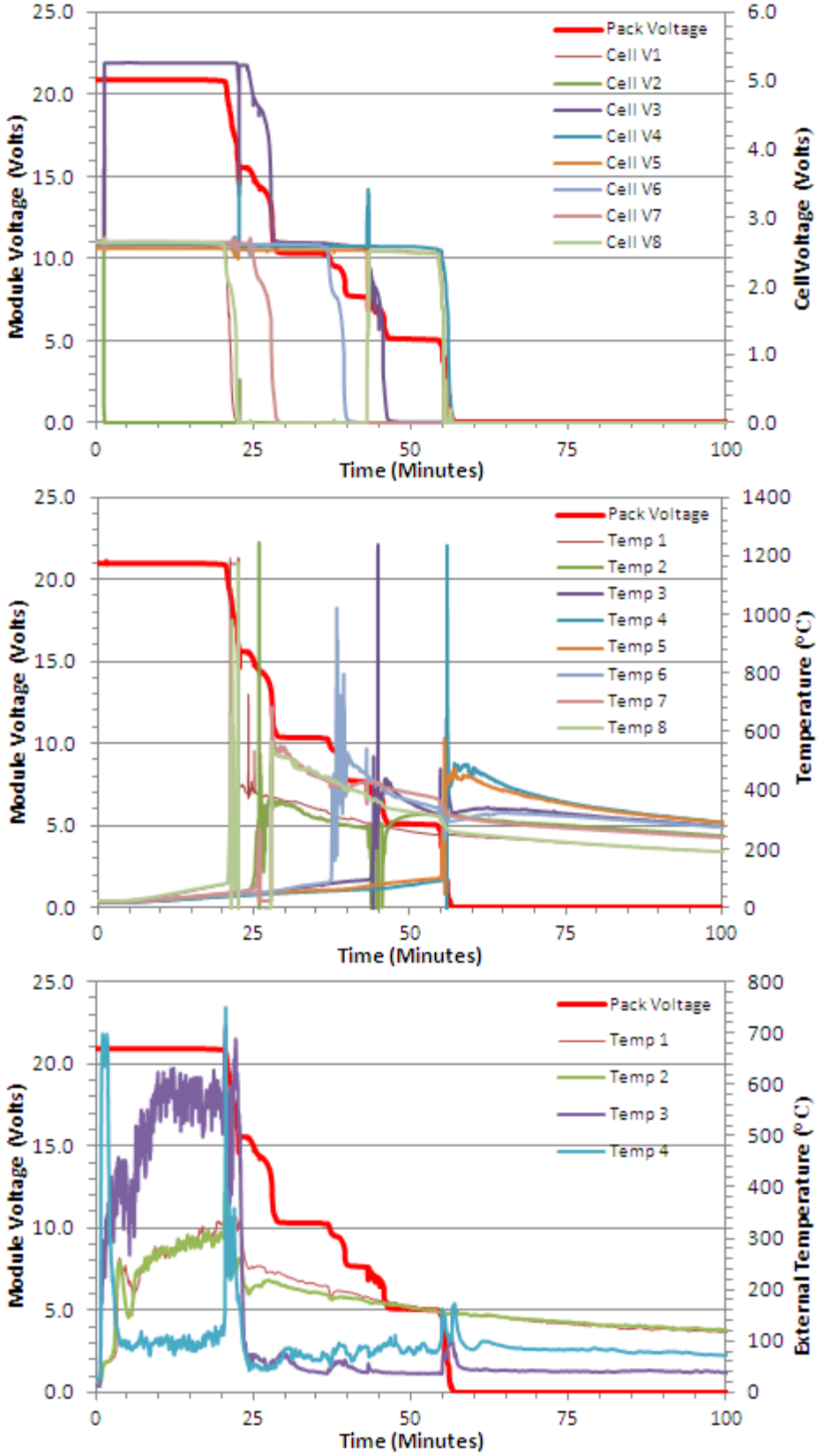

Figure 37: Mark I Module- Water Suppression Test Data

8.5 FM200 Suppression Test

The unique and advantageous properties as a waterless, non-toxic, electrically non-conductive fire suppressant has made FM200 a strong candidate as a fire extinguisher for electrical and battery fires. With an FM200 system currently installed onboard the Sea Jet Advanced Electric Ship Demonstrator (AESD) as the battery compartment's primary fire suppression system, Altairnano has tasked NSWC Crane to test the fire suppressants effectiveness in extinguishing a lithium nano titanate battery fire. For this task Crane forced a single Altairnano Mark I Module to violently vent and initiated an FM200 gas system to extinguish the fire.

8.5.1 Test Setup

Onboard the Sea Jet, the FM200 system has a single discharge nozzle located 6" forward of the geometric center of the two module racks (fore/aft), and slightly 6" port of the ship's keel athwartships. The shortest distance from the nozzle to a battery is 6" above (vertical) and 12" athwartships to port. The nozzles furthest distance to a battery is 60" below (vertical) and 72" fore/aft. Being a highly mobile gas, the efficiency of FM200 in rapidly extinguishing a fire is not dependent upon the exact location of the extinguishing nozzle in relation to the fire, but rather the overall concentration of the suppressant within the room and the temperature of the fire. For this reason a generic location for the exit port of the FM200 nozzle was setup ~70" radially from the battery module and pointed in the opposite direction of the batteries location, Figure 38.

The FM200 system was equipped with two methods of activation. The first is an electronic solenoid that can be externally activated outside the test cell. The second, a failsafe method, is a manual lever on the FM200 tank that could be pulled to activate the gas. Do to the dangers associated with manually pulling the lever during testing; a cord was attached to the lever allowing it to be activated, if the solenoid failed, via a through port on the test chamber wall. Additionally, the test setup included remote ignition of the methanol fire. Further details for the FM200 system can be found in Table 12.

FM200 Chemetron Fire System	
DuPont™ FM-200® CAS Number	431-89-0
Charge Pressure	336 psi @ 70°C
FM200 Gas Weight	150 lbs
Test Room Concentration after Activation	~12% (estimated) by volume
Acceptable Inhalation Concentration (NOAEL)*	10.5% by volume
***No observable adverse effect level (NOAEL)**	

Table 12: FM200 Fire Suppression System Configuration

Figure 38: Mark I Module FM200 Test Setup

8.5.2 Results and Discussion

The Water Extinguishing Test, conducted on Thursday October 21st 2010, demonstrated the effectiveness of 150lbs of FM200 disbursed from a single nozzle within a closed test chamber in suppressing a module battery fire. The FM200 gas was observed to successfully extinguish all fires present at the time of activation. Additionally, no fires were observed, post FM200 activation, during the 45 minute duration where thermal propagation inwards into the battery caused additional cells to vent.

Screenshots from the video of the FM200 test outlining key transitions during the test can be found as Figure 39. After subjecting the module to ~20 minutes of heat from the methanol fire, smoke within the test chamber drastically decreased visibility as shown in Figure 39 frame 19:14. Moments after the test chamber visibility reached a critical point the pack voltage was observed to instantaneously drop 2.6V equivalent to one cell's voltage. This was indicative that a cell had vented or was on the verge of venting and to ensure a visual confirmation of the FM200 systems suppressing the fire the FM200 suppressant was activated. Moments after triggering the extinguisher the fuel fire and some secondary fires on the module, likely to be burning epoxy and or electrolyte, were quickly extinguished with no observable reignitions.

Figure 39: Mark I Module FM200 Test -Test Video Screen Captures

As can be heard on the test video, multiple cells vented immediately following the FM200 activation with no observable flames or detectable heat generated as confirmed by external thermocouples data, Figure 40 (lower graph). The top graph of Figure 40 shows the pack voltage and cell voltages vs. time; however, the cell voltage data and the internal cell thermocouple data sown in the middle graph has apparently been shorted by the flames and is unusable. Although wrapped in fiberglass tape, the flames, as shown in Figure 39 (frame 06:50), likely burnt through the wires shorting them with another surface. This is also evident in the pictures of the Mark I module after FM200 testing, Figure 41.

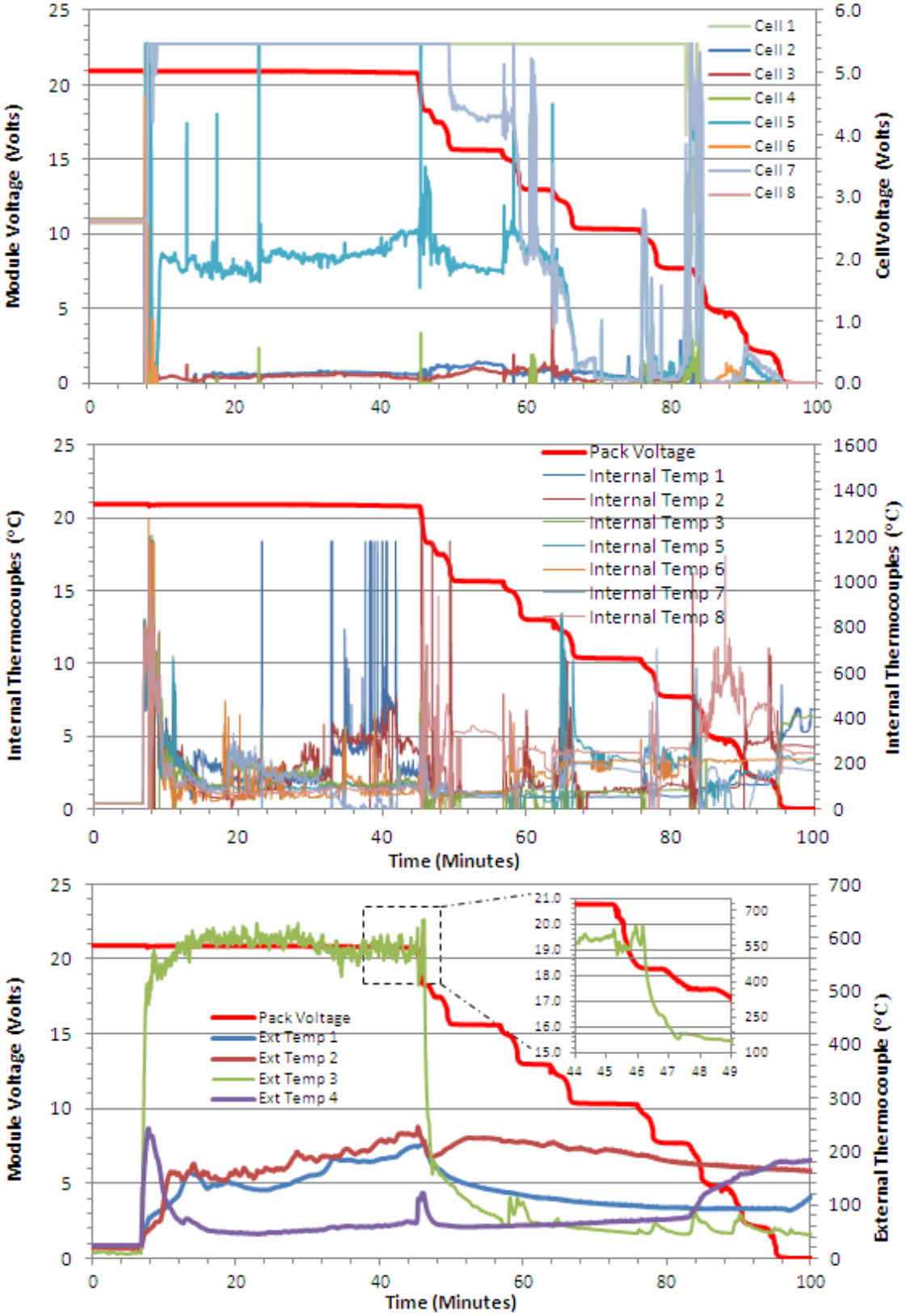

Figure 40: Mark I Module FM200 Test- Data Plots

The DuPont recommended FM200 concentration for extinguishing a Class A fire is 7% v/v whereas our setup intentionally yielded ~12% v/v. The higher concentration was believed necessary due to the above normal flame temperatures the battery fire could potentially provide. During initial exposure of FM200 to high flame temperatures the chemical can decompose into potentially toxic byproducts one of which is hydrofluoric acid (HF). Extensive testing by DuPont has shown that the levels of HF produced in extinguishing typical Class A fires are well below hazardous levels based on the dangerous toxic load (DTL) of HF. Moreover, these levels present no threat to electronics or other sensitive equipment. For fast-growing Class B fires, HF levels may exceed the human DTL depending upon the size of the fire and the volume of the protected area, and HF levels may also present a threat to equipment. In most cases this is a moot point, as the temperatures and levels of toxic combustion products such as carbon monoxide, carbon dioxide, and smoke render the atmosphere toxic and corrosive even before the discharge of FM200.

Figure 41: Fire Suppression Test – FM200 after Test Pictures

8.6 Module Fire Suppression Conclusions

Three types of Fire Suppression methods (CO_2, Water, and FM200) were tested to determine their effectiveness in extinguishing a Mark I Module battery fire. Both the gaseous fire suppressants (FM200 and CO_2) were found to quickly and successful suppress the fire even during subsequent venting events. The water extinguishing test, however, required a much longer period of time to suppress the fire.

The most effective method of fire suppression appeared to be FM200 due to its quick extinguishing capability and the non-toxic nature of the gas (i.e. it is breathable up to ~7%). The CO2 test revealed similar fire suppression performance; however, it would require an extremely fast response by personnel to get the fire under control before it spreads to other batteries. An automated CO2 extinguishing system would efficiently address the problem but adds the risk of asphyxiation.

As previously stated in the FM200 conclusions section, at high temperatures the FM200 can break down to form toxic levels of hydrofluoric acid (HF), but it is likely that other toxic gaseous byproducts from the fire or venting events would be of a primary concern. Due to the stringent regulations of HF byproducts onboard naval ships, it may be of future interest to test for HF concentrations during both the cell venting event and application of FM200.

Appendix

Appendix A: Altairnano Nano-Titanate Cell Specifications Sheet

11 Amp Hour Cell

ALTAIR NANO
charging the energy revolution

Key Features
Based on Altairnano's patented manufacturing process, our products exhibit some of the most exceptional performance in the marketplace today. Replacing graphite with a new high surface area nano lithium-titanate oxide based anode material, Altairnano's products feature unique fast-charge, abuse tolerance, and extreme long life along with cold temperature charging. Some of our key advantages include:

- Large configuration choices
- Greater temperature versatility with ranges of -40° Celsius to 55° Celsius
- Increased level of power (3 times more powerful than existing batteries)
- Long cycle life (exceeding 5,000 charges)
- Fast charge/discharge rates (within 10 minutes)
- Higher levels of operational abuse tolerance than existing batteries

Nano Lithium-Titanate
Battery Cell – 11Ah

CELL SPECIFICATIONS	
Operating temperature range	-40°C to +55°C
Recommended storage temperature	-40°C to +55°C
Nominal voltage	2.3 V
Nominal capacity (1C charge/1C discharge)	11 Ah
Internal discharge impedance (10 sec, DC)	3.5 m ohms typical
Internal charge impedance (10 sec, DC)	3.2 m ohms typical
Internal impedance 1 kHz AC	2.0 m ohms typical
Recommended standard charge/discharge	10 A & constant current
Recommended fast charge	66 A & constant current (110 A max)
Max continuous discharge	110 A
Pulse charge/discharge rate (10 sec pulse)	200 A max
Cell weight	366 g
Physical dimensions (W x H x T)	207 mm x 129 mm x 8 mm
Typical power (10 sec pulse 50% SOC) , at 25°C	400 W & 1100 W/kg
Typical energy, 1C at 25°C	28 Wh & 74 Wh/kg
Expected calendar life at 25°C	20 years
CYCLE LIFE	
At 2C charge & 2C discharge, 100% DOD, 25°C	>12,000 cycles
At 6C charge & 2C discharge, 100% DOD, 25°C	>9,000 cycles
At 1C charge & 1C discharge, 100% DOD, 55°C	>4,000 cycles
RECOMMENDED CUT OFF / CHARGE CUT OFF VOLTAGE	
Recommended cut off voltage in the range -40°C to +30°C	1.5 V
Recommended cut off voltage in the range +30°C to +55°C	2.0 V
Recommended charge cut off voltage at +20°C to +55°C	2.8 V
Recommended charge cut off voltage at -40°C to +20°C	2.9 V

204 Edison Way, Reno, Nevada 89502
tel: 775.856.2500 fax: 775.856.1619
www.altairnano.com

Product Specification Code: C041-0023-011, Dated: 01-22-09

11 Amp Hour Cell

ALTAIR NANO

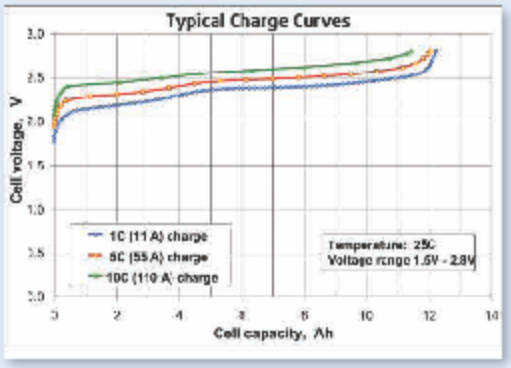

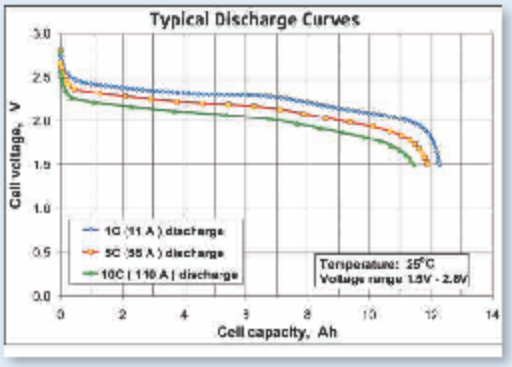

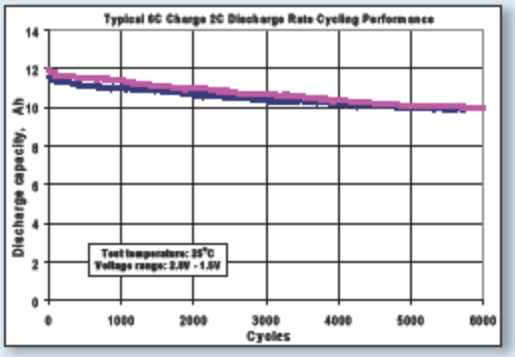

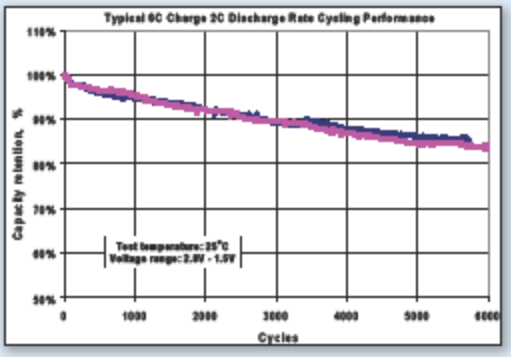

Altairnano Lithium Titanate Battery technology is possibly the safest lithium battery technology available. The cells described in this data sheet have no graphitic anodes which are a weak component in other lithium technologies. However, the electrolyte is flammable. Given the possibility of mechanical or externally caused fire and/or heat damage, the designer of systems using these cells should implement adequate temperature control and physical protection of the cells. Altairnano requires the values on this data sheet not be exceeded in operation or storage. Design of battery systems must follow the instructions and requirements of the companion instruction sheet available from Altairnano dated October 1, 2008 and entitled "Instructions for design and use of Altairnano nLTO battery cells."

Important: All information, including illustrations, is believed to be reliable. Users, however, should independently evaluate the suitability of each product for their particular application. Altairnano makes no warranties as to the accuracy or completeness of the information, and disclaims any liability regarding its use. Altairnano's only obligations are those in the Altairnano Standard Terms and Conditions of Sale for this product, and in no case will Altairnano or its distributors be liable for any incidental, indirect, or consequential damages arising from the sale, resale, use, or misuse of the product. Specifications are subject to change without notice. In addition, Altairnano reserves the right to make changes—without notification to Buyer—to processing or materials that do not affect compliance with any applicable specification.

Altairnano is a registered trademark of Altairnano and its affiliates.

204 Edison Way, Reno, Nevada 89502
tel: 775.856.2500 fax: 775.856.1619
www.altairnano.com

Product Specification Code: C041-0023-011, Dated: 01-22-09

Appendix B: Altairnano Cell Charging Profiles

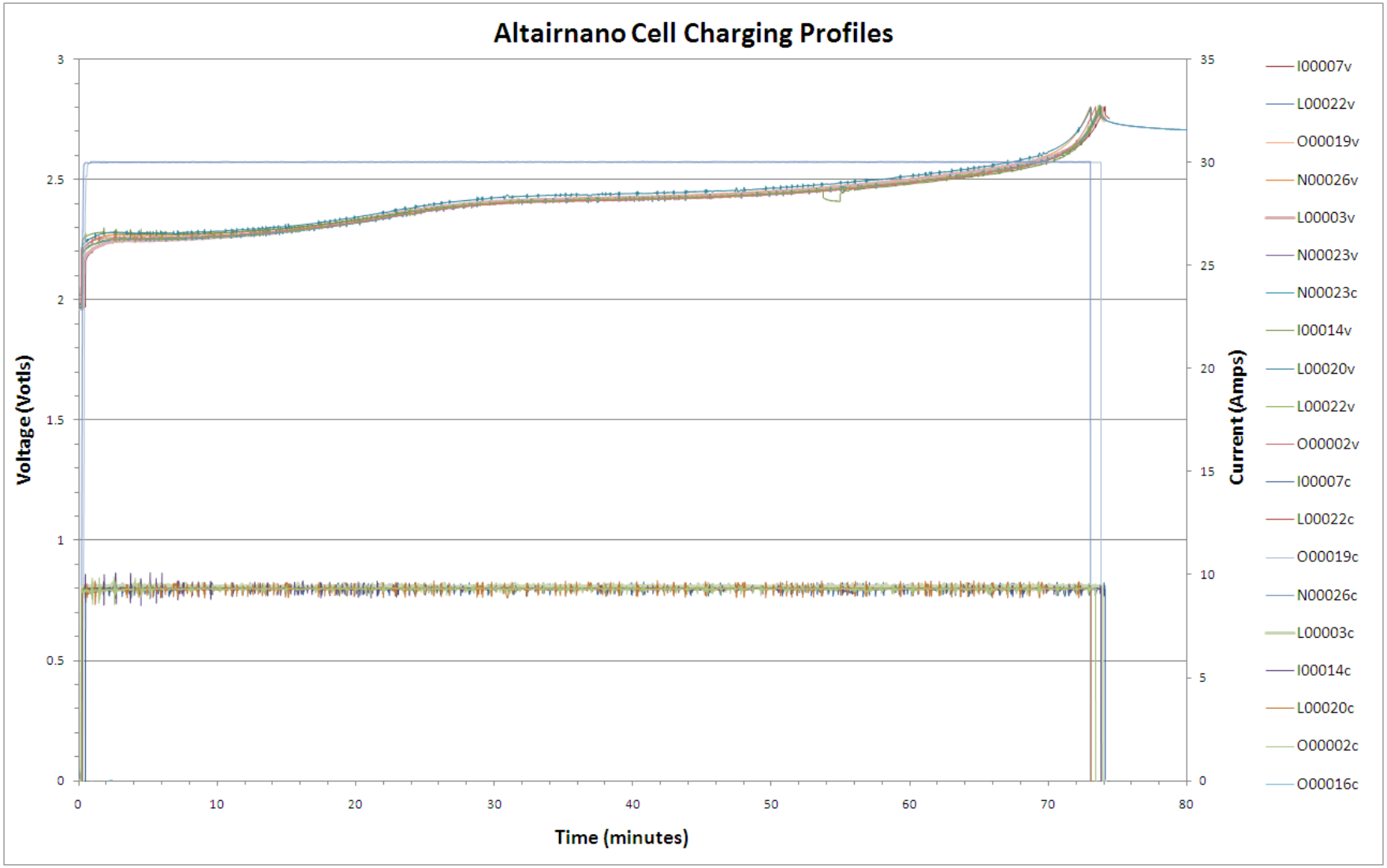

Figure 42: Altairnano Cell Charging profiles

Appendix C: Mark I Module Internal Thermocouple Schematic